Title

Paracrine signalling by pancreatic δ cells determines the glycaemic set point in mice

Journal

Nature Metabolism, 6(1)

ISSN

2522-5812

Authors

Huang, Jessica L

Pourhosseinzadeh, Mohammad S

Lee, Sharon

et al.

Publication Date

2024

DOI

10.1038/s42255-023-00944-2

Peer reviewed

HHS Public Access

Author manuscript

Nat Metab. Author manuscript; available in PMC 2024 March 07.

Published in final edited form as:

Nat Metab. 2024 January ; 6(1): 61–77. doi:10.1038/s42255-023-00944-2.

Paracrine signaling by pancreatic δ cells determines the glycemic set point in mice

Jessica L Huang[1], **Mohammad S Pourhosseinzadeh**[1], **Sharon Lee**[1], **Niels Krämer**[1,2], **Jaresley V Guillen**[1], **Naomi H Cinque**[1], **Paola Aniceto**[1], **Ariana T Momen**[1], **Shinichiro Koike**[3], **Mark O Huising**[1,4]

[1]Department of Neurobiology, Physiology & Behavior, College of Biological Sciences, University of California, Davis, California, USA

[2]Department of Animal Ecology and Physiology, Radboud Institute for Biological and Environmental Sciences, Radboud University, Nijmegen, The Netherlands

[3]Department of Nutrition, University of California, Davis, California, USA

[4]Department of Physiology and Membrane Biology, School of Medicine, University of California, Davis, California, USA

Abstract

While pancreatic β and α cells are considered the main drivers of blood glucose homeostasis through insulin and glucagon secretion, the contribution of δ cells and somatostatin (SST) secretion to glucose homeostasis remains unresolved. Here we provide a quantitative assessment of the physiological contribution of δ cells to the glycemic set point in mice. Employing three orthogonal mouse models to remove SST signaling within the pancreas or transplanted islets, we demonstrate that ablating δ cells or SST leads to a sustained decrease in the glycemic set point. This reduction coincides with a decreased glucose threshold for insulin response from β cells, leading to increased insulin secretion to the same glucose challenge. Our data demonstrate that β cells are sufficient to maintain stable glycemia and reveal that the physiological role of δ cells is to provide tonic feedback inhibition that reduces the β cell glucose threshold and consequently lowers the glycemic set point *in vivo*.

Keywords

δ cells; somatostatin; glucose homeostasis; glycemic set point; glycemia; β cells; insulin secretion; calcium imaging

*Correspondence: mhuising@ucdavis.edu.

AUTHOR CONTRIBUTIONS STATEMENT

Conceptualization, J.L.H. and M.O.H.; Methodology, J.L.H. S.L., and M.O.H.; Software, M.S.P.; Validation, J.L.H., S.L., and M.S.P.; Formal Analysis, J.L.H., S.L., and M.S.P.; Investigation, J.L.H., M.S.P., S.L., N.K., J.V.G., N.C., P.A., A.T.M., and S.K.; Writing - Original Draft, J.L.H and M.O.H; Writing - Review & Editing, J.L.H., M.S.P., and M.O.H.; Visualization, J.L.H., M.S.P., and M.O.H.; Supervision, M.O.H.

COMPETING INTERESTS STATEMENT

M.O.H. received grant support from Crinetics, Inc. to evaluate proprietary somatostatin-related compounds. None of this work is discussed in this paper. All other authors declare no competing interests.

Blood glucose levels are maintained within a narrow range around the glycemic set point, defined as a fixed level of blood glucose that the body aims to achieve in between meals[1]. Glucose homeostasis changes during postnatal development in rodents, but is generally stable within an adult individual throughout the lifespan unless disrupted by disease. In humans, this set point is around 90 mg/dL (approximately 5 mM)[2], while in mice it is around 120-140 mg/dL (approximately 7-8 mM)[3-5]. Tight regulation of blood glucose homeostasis is crucial, as chronic hyperglycemia causes a plethora of long-term complications, while hypoglycemia is acutely life-threatening.

The hormones released by pancreatic islets are known to play critical roles in blood glucose homeostasis. Under prandial conditions when glycemia is high, β cells secrete insulin to signal for the uptake and storage of glucose. Conversely, under post-prandial conditions when glycemia is low, α cells secrete glucagon to stimulate hepatic glucose production. There is increasing evidence that paracrine glucagon signaling also amplifies glucose-stimulated insulin secretion (GSIS) by directly stimulating β cells [6-12]. This suggests that paracrine actions of glucagon stimulate GSIS during the prandial state, while systemic actions of glucagon are responsible for its counterregulatory function during the post-prandial state[13]. The third major cell type of the islet is the δ cell, which releases somatostatin (SST) to inhibit both β and α cells.

The glycemic set point is often attributed to the crossover point between β and α cell glucose response[4,14]. However, the question of where and how the glycemic set point is determined continues to elicit debate. The central nervous system (CNS) is another key regulator of blood glucose homeostasis [15,16], with glucose-sensing neurons present throughout the hypothalamus, including in the ventromedial nucleus, paraventricular nucleus, and lateral hypothalamus[17]. Moreover, glucose sensing defects at these sites contribute to type 2 diabetes (T2D). The CNS has also been demonstrated to be capable of lowering glycemia in an insulin-independent manner[18-20]. These observations indicate that the CNS is important for controlling glycemia. However, there is compelling evidence that the pancreatic islet is the major glucostat of the body in between meals. Transplanting islets from different donor species into diabetic nude mice causes recipients to re-establish a glycemic set point matching that of the donors, demonstrating that islets without their regular innervation are both sufficient for normoglycemia and responsible for the glycemic set point[21]. More recently, an experiment where human, mouse or macaque islets were transplanted into diabetic nude mice demonstrated that the glycemic set point is dependent on paracrine interactions within the transplanted islets[4].

These experiments provide evidence that paracrine signals within the pancreatic islet are key players in establishing the glycemic set point, but did not address the potential paracrine contribution of δ cells to this set point. β cells in mice do not respond to glucose until around 7-8 mM glucose [22], and glucagon secretion from α cells in mice is maximally suppressed at 7 mM glucose [22,23]. Therefore, at the glycemic set point, β cells are not yet activated, and α cell activity is at a nadir. In contrast, δ cells are active over a range of glucose levels, secreting SST at glucose levels as low as 3 mM with amplification at higher glucose levels [24-26]. Inhibition of insulin and glucagon secretion by SST under stimulated conditions is well-established [26-29] and knockout of SST has been shown to augment GSIS

and arginine-stimulated glucagon secretion [23,29,30]. However, the physiological contribution of δ cell-secreted SST to the glycemic set point has not been established.

Previous evidence indirectly points to a role of δ cell-derived SST in determining the glycemic set point through communication with β cells. Our lab established that β cells co-secrete the hormone Urocortin 3 (UCN3) with insulin, and that within the islet UCN3 acts solely on δ cells to stimulate SST secretion [24]. The onset of UCN3 expression in approximately 2-week old mice is associated with an increase in the glycemic set point[3,31]. Premature induction of UCN3 in neonatal mice caused a comparable and premature increase in glycemia, while continued induction of UCN3 after onset of endogenous UCN3 expression had no further effect, demonstrating that the increased set point observed in young mice is caused by the onset of UCN3 expression. UCN3 expression is also downregulated in T2D, which leads to reduced SST secretion to allow for a compensatory increase in insulin in the face of peripheral insulin resistance [24,32,33]. Restoring UCN3 expression and the ensuing SST feedback suppressed insulin secretion in diabetic *ob/ob* mice, aggravating hyperglycemia[24]. From these observations, we predicted that δ cell feedback via the local release of endogenous SST helps determine the glycemic set point[34].

Here we set out to rigorously test the hypothesis that SST contributes to the glycemic set point. We do so with three complementary mouse models of removing SST-mediated inhibition of β cells in adult mice that consistently lead to an immediate and sustained decrease of 20-30 mg/dL in blood glucose. We demonstrate that the effect on the glycemic set point is specific to the loss of pancreatic δ cell-derived SST, ruling out contributions from non-pancreatic sources of SST to this phenotype. We then demonstrate that this acute drop in the glycemic set point is due to increased insulin secretion by measuring plasma insulin *in vivo* and secreted insulin *ex vivo*. Parallel pancreatic α cell ablation experiments do not shift the glycemic set point, confirming prior published observations[35-37]. Furthermore, quantifying β cell calcium responses within intact islets over time revealed a decreased glucose threshold for β cell response of approximately 1 mM glucose in the absence of δ cells. This reduced β cell glucose threshold closely matches the 20-30 mg/dL reduction in the glycemic set point observed *in vivo* upon interruption of δ cell function in multiple parallel experiments. We conclude that δ cells shift the glycemic set point through their local inhibitory interactions with β cells, modulating the glucose threshold for insulin secretion.

RESULTS

Absence of somatostatin lowers the glycemic set point

To investigate the contribution of SST to the glycemic set point, we used mice with the *Sst*-IRES-Cre transgene, which disrupts SST expression[38]. Homozygous *Sst*-IRES-Cre mice (*Sst*-Cre$^{TG/TG}$) crossed to a floxed YFP reporter (lsl-YFP) allowed for identification of δ cells with YFP. This confirmed that SST is absent but δ cells remain in *Sst*-Cre$^{TG/TG}$ mice, while SST is present in δ cells of heterozygous littermates (*Sst*-Cre$^{+/TG}$ x lsl-YFP) (Fig. 1A and 1B). *Sst*-Cre$^{+/TG}$ mice had slightly reduced *Sst* transcript levels compared to *Sst*-Cre$^{+/+}$ mice as previously reported[38], but it was not statistically significant, while *Sst* transcript was absent in *Sst*-Cre$^{TG/TG}$ mice (Fig. 1C). We took advantage of these effectively *Sst*-null mice to test the hypothesis that the absence of SST would decrease the glycemic set point.

To determine whether the absence of SST affects glycemia, we conducted weekly glucose measurements on the mice. Both male and female *Sst*-Cre$^{TG/TG}$ mice exhibited lower non-fasting glucose levels compared to control *Sst*-Cre$^{+/TG}$ mice of the same sex (Fig. 1D, 1E), with no significant changes in body weight (Extended Fig. 1A, 1B). We then investigated changes in fasting and challenged glycemia using an intraperitoneal (IP) glucose tolerance test (GTT). Neither sex exhibited significant changes in glucose tolerance (Fig. 1F, 1G). While plasma insulin levels were significantly higher in male *Sst*-Cre$^{TG/TG}$ mice relative to male *Sst*-Cre$^{+/TG}$ mice (Fig. 1H), there was no significant difference in the fold change in insulin levels when we compared plasma insulin levels before and after glucose administration (Fig. 1I). There was no significant difference in plasma insulin levels or fold change in insulin between female *Sst*-Cre$^{+/TG}$ and *Sst*-Cre$^{TG/TG}$ mice (Fig. 1J, 1K). However, islets from female *Sst*-Cre$^{TG/TG}$ mice secreted significantly more insulin under 11 mM glucose (Fig. 1L, 1M), matching the phenotype reported for *Sst*$^{-/-}$ mice[29].

Specific ablation of pancreatic δ cells by diphtheria toxin

Although *Sst*-Cre$^{TG/TG}$ mice have lower non-fasting glycemia and can secrete more insulin in response to the same glucose challenge, the absence of a difference in glucose tolerance suggests that there may be some compensation for the constitutive absence of SST from birth. We therefore turned to a model that would allow us to ablate δ cells and SST signaling within the islet at a time of our choosing using diphtheria toxin (DT). We generated *Sst*-Cre$^{+/TG}$ x Rosa-lsl-iDTR mice (*Sst*-Cre x lsl-DTR mice) expressing the DT receptor (DTR) in SST-expressing cells that would be ablated upon DT administration. *Sst*-Cre$^{+/TG}$ mice were used for these experiments, as *Sst*-Cre$^{TG/TG}$ mice already have lower glycemia (Fig. 1). We confirmed complete δ cell ablation in DT-treated *Sst*-Cre x lsl-DTR mice, while β and α cell numbers did not significantly change relative to saline (SAL)-treated *Sst*-Cre x lsl-DTR or non-floxed littermate controls (Fig. 2A, 2B). *Sst* mRNA levels were reduced by approximately 40-fold after ablation, while *Ins2* and *Gcg* levels were unaffected (Fig. 2C). Pancreatic δ cells remained ablated even 3 months after DT administration (Fig. 2D), consistent with reports that they are long-lived cells with a low turnover rate [39]. Furthermore, control islets secreted detectable SST in the presence of 5.5 mM glucose alone that was amplified upon addition of 100 nM ghrelin, while SST secreted from δ cell-ablated islets was below the limit of detection even in the presence of ghrelin (Fig. 2E).

SST is also expressed in other tissues throughout the body, primarily the stomach, duodenum, and throughout the brain. We collected these tissues to assess the extent of ablation in these areas. Both qPCR and staining for SST revealed that gastric D cells were lost upon acute ablation, but began recovering within two weeks and recovered completely within three months (Fig. 2F, 2G). Duodenal D cells were present in both control and ablated mice, which was reflected by partial reduction in *Sst* transcript level following DT administration that completely recovered by 2 weeks (Fig. 2H, 2I). The at best transient loss of D cells in the gastrointestinal tract followed by recovery is in line with the well-established ability of the gastrointestinal mucosae to self-renew within a relatively short period[40]. In the hypothalamus, there was no significant difference in *Sst* transcript (Fig. 2J). Imaging whole brain slices from *Sst*-cre x lsl-tdTomato x lsl-DTR mice, in which SST-expressing cells are labeled with both tdTomato and DTR, revealed no significant

differences between ablated mice and controls in the number of tdTomato+ neurons in the brain or in specific regions like the hypothalamus and cortex (Fig. 2K, 2L). This suggests that the dose and frequency of DT administration that we used spared SST-expressing neurons in the brain.

δ cell ablation lowers the glycemic set point

To determine the effect of δ cell ablation on glycemia, we conducted weekly glucose measurements on the mice, with daily measurements throughout the period of injection. In both sexes, glucose levels between groups were indistinguishable prior to δ cell ablation (Fig. 3A, 3B). Following IP injection of DT, *Sst*-Cre x DTR mice of both sexes immediately exhibited a significant and lasting decrease in glucose levels compared to control littermates. *Sst*-Cre only and SAL-treated *Sst*-Cre x lsl-DTR mice were comparable in response as controls (Extended Fig. 2). The difference in basal glycemia between the groups remained even after 3 months. Given that the glycemic set point remains lower even after 3 months and only the δ cells remain completely absent at that time point (Fig. 2), this indicates that the sustained change in the glycemic set point in these mice can be specifically attributed to pancreatic δ cell ablation.

We also observed that DT-treated *Sst*-Cre x lsl-DTR males had a lower body weight relative to controls (Extended Fig. 3A, 3B). This brought up the possibility that lower food intake contributed to the decreased glycemia. Ablation of SST-expressing neurons specifically in the tuberal nucleus of the hypothalamus has previously been demonstrated to decrease food intake[41]. While we did not detect a loss of SST-expressing neurons, we still measured food intake in DT-treated *Sst*-Cre x lsl-DTR mice and *Sst*-Cre littermates without the lsl-DTR transgene and observed no significant changes (Extended Fig. 3C). In combination with the lack of detectable SST-expressing neuron loss in the brain, this does not support the loss of SST neurons in regions responsible for feeding such as the tuberal nucleus as a possible mechanism for the modest difference in body weight of male mice.

To determine the effect of δ cell ablation during glucose stimulation, we conducted IPGTTs on the mice before and after administration of SAL or DT. There was no significant difference between the glucose tolerance of the different groups of mice prior to δ cell ablation (Fig. 3C, 3E). IPGTTs performed 36 hours after the last administration of DT revealed significantly improved glucose tolerance in δ cell-ablated mice (Fig. 3D, 3F). GTT experiments performed 3 months after ablation demonstrated that the increased glucose tolerance remains (Extended Fig. 3D, 3E), consistent with δ cells remaining ablated during this time.

Given that δ cell ablation would decrease SST tone and remove its local inhibition of β cells, we hypothesized that the decrease in the glycemic set point and increase in glucose tolerance would both be the result of an increase in glucose-stimulated insulin secretion (GSIS). To test this hypothesis, we measured plasma insulin in fasted DT-treated *Sst*-Cre x DTR mice and controls before and 15 minutes after IP injection of glucose. Fasting and glucose-stimulated plasma insulin levels were comparable between groups in both sexes prior to ablation (Fig. 3G, 3J). After δ cell ablation, there was a slight but non-statistically significant increase in glucose-stimulated plasma insulin levels in DT-treated males (Fig.

3H). However, there was a significant increase in the fold-change of plasma insulin after ablation, as determined by dividing plasma insulin levels 15 minutes after glucose injection by baseline plasma insulin levels in each mouse (Fig. 3I). No differences in plasma insulin levels were observed in females (Fig. 3K, 3L).

To confirm our *in vivo* findings *in vitro*, we compared static GSIS in the presence and absence of δ cells in isolated intact islets. This revealed a consistent increase in GSIS at glucose levels mildly or moderately above the β cell glucose threshold, reaching significance at 16.8 mM glucose in islets from both sexes (Fig. 3M, 3N). Thus, GSIS increases in the absence of pancreatic δ cells in an islet autonomous manner.

To obtain higher temporal resolution of changes in the glycemic set point, we placed continuous glucose monitors on the mice to measure glucose with 5-minute resolution as described before[24]. Within 12 hours of a single dose of DT, the blood glucose levels of *Sst*-Cre x DTR mice began to drop and remained steady for the duration of the experiment (Fig. 3O). This confirmed that the changes observed through the weekly glucose measurements indeed reflected an acute and lasting change in the glycemic set point of the mice.

Somatostatin mediates the changes in the glycemic set point

We next employed the *Sst*-Cre$^{+/TG}$ x *lsl-Gα$_i$-DREADD* model (*Sst*-Cre x Gi-DREADD). In this mouse model, SST-expressing cells express Gi-DREADD, a modified M4 muscarinic receptor that can be activated by administration of clozapine-N-oxide (CNO). As a $G_{\alpha i}$-coupled receptor, Gi-DREADD activation leads to decreased adenylyl cyclase activity and subsequent decrease in cAMP levels, which ultimately inhibits secretion. This allowed us to acutely inhibit δ cell activity and SST secretion with CNO, while keeping δ cells intact and allowing for reversal of δ cell inhibition upon removal of CNO. IP administration of CNO (1 mg/kg) led to a significant decrease in non-fasting blood glucose levels 1 hour or 30 minutes after injection in male and female *Sst*-Cre x Gi-DREADD mice, respectively, relative to littermate controls without Gi-DREADD or injected with SAL (CTRL) (Fig. 4A, 4B). This is consistent with the decrease in glucose levels seen in δ cell-ablated mice. By 24 hours after CNO administration, there was no significant difference in non-fasting glucose levels between the CTRL and CNO groups in either sex (Fig. 4A, 4B). IPGTTs performed in independent experiments 1 hour after CNO administration showed that inhibiting δ cell activity also improved glucose tolerance (Fig. 4C, 4D). These data further support the contribution δ cell activity to the glycemic set point.

Ablation of islet δ cells decreases the glycemic set point

To determine whether pancreatic δ cell ablation alone is sufficient to decrease glycemia, we performed islet transplant studies. *Sst*-Cre$^{+/TG}$ x lsl-DTR or *Sst*-Cre$^{+/TG}$ only mice were used as donors, while WT littermates without *Sst*-Cre nor DTR were used as recipients (Fig. 5A). First, we induced stable hyperglycemia by ablating β cells within the WT recipients using streptozotocin at multiple low doses (50 mg/kg) for 5 consecutive days. We then isolated islets from the donor mice and transplanted the islets under the kidney capsule of the recipient mice to re-establish normoglycemia. We chose a relatively low dose of 100 islets per mouse to avoid a lower than normal glucose setpoint that could result from the

transplantation of a larger number of islets than necessary to restore normoglycemia[42]. This arrangement ensured that the glycemic set point would be determined by the transplanted islets containing DTR-expressing δ cells, with the additional benefit that we could transplant the same number of islets from a single donor into a single recipient. Since the WT mice's endogenous tissues do not express DTR, none of the other SST-expressing cells would be affected by DT. Therefore, any change in the glycemic set point following DT administration would have to be caused by the loss of transplanted δ cells. We indeed observed a stable decrease in blood glucose levels following DT administration to mice that received *Sst*-Cre x lsl-DTR islets but not mice that received *Sst*-Cre only islets (Fig. 5B, 5C). We confirmed that δ cells remained present in DT-treated mice that received *Sst*-Cre only islets (Fig. 5D, 5F) and that δ cells were ablated in DT-treated mice that received *Sst*-Cre x lsl-DTR islets (Fig. 5E, 5F) as assessed in the retrieved transplants at the conclusion of the experiment. Plasma insulin levels were not collected at that time Our transplantation experiment was designed to follow plasma glucose levels by repeated measure and was likely not adequately powered to determine a potential difference of a single endpoint measurement such as plasma insulin. The expression of the maturity marker UCN3 in the transplanted β cells of both groups confirmed they maintained their mature β cell identity (Fig. 5D, 5E). This demonstrates that selective pancreatic δ cell ablation, with no possible ablation of SST-expressing cells elsewhere in the body, is sufficient to decrease the glycemic set point.

α cell ablation does not affect basal glycemia

The role of α cells in amplifying GSIS in the prandial state is increasingly appreciated. Although glucagon is generally thought of as a hormone that acts to raise glucose levels, it also potentiates GSIS to bring glucose levels down in the prandial state[7-9,11]. Furthermore, a comprehensive and elegantly executed paper establishing that the glycemic set point is set by paracrine interactions within the islet concluded that the underlying mechanism was paracrine crosstalk between β and α cells[4]. However, mouse models of α cell ablation generally demonstrated no change in glycemia nor insulin secretion[35-37], with the exception of moderately decreased GSIS from a pancreas perfusion[7]. Thus, we considered it important to directly compare the effect of δ and α cell ablation on glycemia and insulin secretion. We set up *Gcg*-CreER x lsl-DTR mice to enable DT-mediated α cell ablation, with the *Gcg*-CreER line chosen for its superior and more specific labeling of α cells[43]. Successful α cell ablation was confirmed by immunofluorescence, qPCR, and decreased glucagon secretion (Fig. 6A-6D). Pancreatic α cell ablation did not significantly affect the glycemic set point, glucose tolerance based on AUC, or plasma insulin levels in mice of both sexes (Fig. 6E-6K). These findings are in close agreement with previous studies that investigated changes in glycemia after α cell ablation[35-37] and confirm that ablating α cells in mice does not alter non-fasting blood glucose levels, in contrast to our δ cell ablation experiments using the same methodology.

Since SST inhibits glucagon secretion, we also examined the effect of δ cell ablation on glucagon secretion. We stimulated α cells with 100 nM epinephrine under low glucose and observed significantly increased glucagon secretion in islets without δ cells, suggesting that loss of paracrine SST from δ cell ablation does indeed disinhibit α cells in the face

of concurrent and direct stimulation (Extended Fig. 4A). This is in line with other studies that have established the role of δ cells in restraining α cell glucagon release[23,26,30]. To determine glucagon contribution to the increased GSIS observed in Fig. 3M and 3N, we measured glucagon concentration from the same samples. A pattern of higher glucagon secretion in the absence of δ cells was observed (Extended Fig. 4B, 4C). This suggests that the absence of local SST signaling leads to reduced inhibition of α cell activity under high glucose, which may contribute to the increased GSIS observed at glucose levels well above the glucose threshold for insulin secretion.

δ cell ablation decreases the β cell glucose threshold

To assess mechanistically how δ cell ablation affects β cell glucose response at the single cell level, we turned to calcium imaging. As calcium is necessary for insulin secretion, changes in intracellular calcium levels are an excellent proxy for insulin secretion. Calcium imaging using the genetically-encoded GCaMP6s sensor allows for single-cell resolution and subsequent fixation and *post hoc* immunofluorescent staining to allow for validation of the identity of the recorded cells. To this end, we generated quadruple transgenic mice expressing *MIP*-Cre/ERT x *Sst*-Cre x lsl-DTR x lsl-GCaMP6 (Fig. 7A). In this line, mice constitutively express both DTR and GCaMP6 in SST-expressing cells. After DT-mediated δ cell ablation, tamoxifen administration to the mice allows for the translocation of Cre/ERT to the nucleus, activating GCaMP6 expression in insulin-expressing β cells. The simultaneous induction of DTR in β cells does not lead to β cell ablation as DT is no longer administered. This strategy allows us to ablate δ cells, then observe β cell calcium response. Due to the complexity of the cross, we used a mix of SAL-treated *MIP*-Cre/ERT x *Sst*-cre$^{+/TG}$ x DTR x GCaMP6 mice and DT-treated mice expressing *MIP*-Cre/ERT x GCaMP6 with or without DTR or *Sst*-cre as controls. We hypothesized based on our observations that the loss of δ cells would shift the β cell glucose threshold to the left. To test this hypothesis, we performed glucose step experiments starting below the β cell glucose threshold at 4 mM glucose and increasing in 1 mM increments every 10 minutes, observing islets with and without δ cells simultaneously in the same microfluidic chamber. After each trace, islets were fixed to confirm the absence of δ cells in ablated islets and to ensure that each GCaMP6 expressing cell was insulin-positive via *post hoc* whole mount immunofluorescence.

To analyze β cell calcium response, we defined the activity threshold as the half-maximum of the signal for each individual β cell. We then determined the glucose level at which each cell first reaches that threshold. In control islets with intact δ cells, individual β cells began responding shortly after exposure to 6-7 mM glucose, with a synchronized response between most β cells by 8-9 mM glucose (Fig. 7B, Extended Fig. 5-7A, Supp. Video 1). Presence of δ cells was confirmed by a *post hoc* stain (Fig. 7C). In islets with ablated δ cells, individual β cells began to respond shortly after exposure to 5-6 mM glucose, with a synchronized response by 7-8 mM glucose (Fig. 7D, Extended Fig. 5-7B, Supp. Video 1) and absence of δ cells confirmed by a *post hoc* stain (Fig. 7E). Quantified across over 1000 β cells from at least 10 islets per mouse in 3 pairs of mice, the β cell glucose threshold in islets without δ cells was on average 1 mM glucose lower and significantly different from islets with intact δ cells (Fig. 7F, 7G). We also conducted traces in which there was a return to 5 mM

glucose between each step to ensure that any responses seen at a specific glucose level could not potentially be a delayed response to the previous glucose level. Here too islets from δ cell-ablated islets responded at a lower glucose level than control islets (Extended Fig. 5-6C, 5-6D).

To determine whether the shift in calcium response also represents a shift in insulin secretion, we simultaneously imaged β cell calcium activity while collecting the outflow to measure insulin secretion. This demonstrated that β cells secrete insulin at a higher amplitude in islets without δ cells (Extended Fig. 8). From these experiments, we concluded that δ cell ablation decreases the glucose threshold at which β cells become active and observe that the 1 mM (18 mg/dL) decrease in the glucose threshold is similar to the approximately 20-30 mg/dL decrease in the glycemic set point observed in mice *in vivo*.

DISCUSSION

SST has long been known to be capable of inhibiting both β and α cells[44-46]. SST secretion from δ cells has been proposed to prevent excess insulin secretion[24,34] and demonstrated to inhibit glucagon secretion in the prandial phase[23,26]. However, the physiological contribution of local δ cell-mediated feedback on the glycemic set point has not been addressed. Here we resolve this by demonstrating that δ cells determine the glycemic set point in mice by modulating the glucose threshold of pancreatic β cells. Mice exhibit an immediate and sustained decrease in basal blood glucose levels upon δ cell ablation. Male mice also exhibit an increase in glucose tolerance that occurs due to an increase in the fold-change of plasma insulin secreted in response to glucose. Static secretion assays of isolated islets confirmed increased GSIS in both sexes. This suggests that there may be other physiological factors in female mice that prevent the increase in plasma insulin levels seen in male mice; for example, females are protected from systemic insulin resistance compared to males[47,48], which may explain why they did not exhibit changes in glucose tolerance. The use of *Sst*-Cre x Gi-DREADD mice showed that inhibiting δ cell activity is sufficient to decrease glycemia and increase glucose tolerance. Furthermore, we isolated the effects of δ cell ablation within the islet through transplant experiments in which *Sst*-Cre or *Sst*-Cre x lsl-DTR islets were transplanted under the kidney capsule of wild-type mice. Ablation of δ cells within transplanted islets without ablation of any other SST-expressing cells in a syngeneic islet transplantation model led to a decrease in non-fasting blood glucose levels. Together, our observations quantify the impact that islet δ cells have on maintaining glucose homeostasis as indicated by *in vivo* islet transplantation (Fig. 5), as well as *in vitro* and *in vivo* observations from multiple mouse models (Fig. 1-4). Single-cell calcium imaging revealed that in the absence of δ cells, β cells respond to lower levels of glucose, demonstrating increased glucose sensitivity. The consistency with which β cells respond at a 1 mM lower glucose level in islets without δ cells is in line with the approximately 1 mM decrease in blood glucose levels. Altogether, our data obtained via multiple complementary models demonstrate that removing paracrine SST secretion from δ cells within the pancreatic islet leads to a decreased glycemic set point (Fig. 8). This decrease is likely driven by de-repression of insulin secretion, although the plasma insulin differences observed upon ablation of endogenous δ cells are modest (Fig. 3). *In vitro*, we demonstrated significant changes in 1-hour static insulin secretion only under high

glucose conditions where SST likely inhibits β cell cAMP levels in addition to intracellular Ca^{2+}. Nevertheless, based on the preponderance of our observations, we consider a modest increase in insulin secretion to be by far the most plausible mechanistic explanation for the consistent reduction in the glycemic set point that illustrates the physiological impact of pancreatic δ cells.

One *Sst*-null mouse model was previously observed to have increased non-fasting blood glucose levels at 3 weeks of age[49]. Another *Sst*-null mouse model has also been noted to have lower blood glucose levels but no differences in non-fasting insulin levels[50]. These mice also display no differences in glucose tolerance relative to wild-type mice but a slight elevation in fasting insulin[51,52], matching our observations in *Sst*-$Cre^{TG/TG}$ mice. Thus, it is indeed likely that there are compensatory effects when SST is constitutively absent. Another paper using the same *Sst*-Cre x lsl-DTR model did not see a change in glucose levels upon DT administration[53]. However, the data were based on 3 male mice per group. The data may also reflect fasting blood glucose levels, which would agree with our data showing no difference in fasting glucose levels in DT-treated *Sst*-Cre x lsl-DTR males.

Because SST exerts many possible actions at different sites throughout the body, including but not limited to the brain, stomach, and intestines, we took care to isolate the contributions of SST within pancreatic islets. The duodenum is unlikely to contribute since there is little ablation and complete recovery within 2 weeks. The stomach is also unlikely to contribute since it recovers within 3 months, at which point the mice still exhibit a decreased glycemic set point. Furthermore, D cells in the stomach inhibit gastric secretion by inhibiting gastrin release[54,55] and suppressing gastric motility[56] and emptying[57]. Collectively, the combined effects of D cells would decrease the nutrient absorption rate and lead to increased circulating nutrients, at least post-prandially. Therefore, the observed reduction of blood glucose upon δ cell ablation or inhibition is inconsistent with reduced D cell function, but consistent with reduced δ cell-mediated inhibition of β cells.

Since the hypothalamus plays an important role in energy metabolism, it is possible that ablating SST-expressing neurons, which have been implicated in food and water intake[58,59], would contribute to the decreased glycemia. We ruled out potentially confounding effects of hypothalamic SST neuron ablation by observing no changes in the number of SST-expressing neurons after ablation nor in food intake between mice with and without δ cells. Our observations are consistent with a recent paper reporting that specifically ablating SST-neurons in the hypothalamus by stereotaxic injection of DTA, the catalytic unit of DT, had no effect on blood glucose or non-fasting insulin levels[60]. Furthermore, specific ablation of δ cells in islets transplanted into WT mice with no other sites of SST ablation replicated the decrease in the glycemic set point. When taken together, our observations support the conclusion that the rapid and sustained reduction in the glycemic set point we observe upon DT administration is attributable to the loss of pancreatic δ cells.

A recent paper reported that pancreatic δ cell ablation leads to neonatal death, which the authors attributed to severe hypoglycemia caused by excess insulin secretion in the absence of intraislet feedback inhibition by SST[61]. However, the approach in that paper depended on the same Sst-Cre driver we used here, in combination with the lsl-DTA

mouse[62]. This strategy leads to the expression of the catalytic subunit of DT constitutively from the moment the *Sst* promoter is activated and would have caused immediate and cell-autonomous loss of cells across the entire SST expression domain, including the disruption of the growth hormone axis and gastrointestinal control, and cause broad loss of neurons across the CNS (Fig. 2). The lack of specificity in the Sst-Cre x lsl-DTA mouse model would lead to many confounds that were not controlled for and that alone or in combination could easily lead to a failure to thrive and neonatal death. In contrast, by expressing DTR in combination with a careful peripheral dosing regimen of DT in adult mice, we have established temporal control over the onset of ablation, with sustained and restricted ablation to δ cells in the pancreas while sparing the CNS. The conclusion that the absence of δ cells leads to neonatal death is inconsistent with multiple mouse models, including our δ cell ablation model, multiple *Sst*-null mice[29,38,50], and also *Hhex*-KO mice that do not develop pancreatic δ cells due to absence of the essential transcription factor HHEX that is required for δ cell formation[63]. These mice are all viable, making it unlikely that δ cell ablation is primarily responsible for the early perinatal lethality of *Sst*-Cre x lsl-DTA mice. Indeed, we have previously demonstrated that δ cell-dependent feedback inhibition of insulin secretion in mice depends on the onset of UCN3 expression in most β cells between 2-3 weeks after birth. It is the completion of this paracrine β-to-δ-to-β feedback loop that drives the noted increase in glucose set point that occurs at this age[24]. Our current data here extend those earlier observations to demonstrate that pancreatic δ cell ablation leads to modestly increased insulin secretion, which leads to decreased glucose levels that stabilize around a new and lower glycemic set point.

Our data demonstrating that α cell ablation has no effect on the glycemic set point agrees with two previous studies that α cell ablation does not affect glycemia in mice[35,36]. While α cells undoubtedly play an important role in both the counterregulatory response through systemic action and the stimulation of GSIS through paracrine action in the prandial phase, their contribution appears to be dispensable around the non-fasting glycemic set point in mice. However, the paracrine interactions and islet interactions are substantially different between species[64-67] and it remains plausible that α cells contribute more directly to the determination of the glycemic set point in human islets[4].

Since these experiments were all performed in the context of healthy mice, it would be interesting to observe the effect that the absence of δ cells can have in models of diabetes, such as in mice on a high fat diet (HFD). It has previously been demonstrated that δ cell activity in HFD-fed mice is impaired[39] and that SST secretion from islets is reduced[68], with similar results also seen in *ob/ob* mice[24]. It is likely that this reduction in SST secretion is related to the drop in β cell UCN3 expression that may reflect a compensatory mechanism to allow for increased insulin secretion in response to rising insulin demand, as restoring UCN3 aggravates hyperglycemia in *ob/ob* mice[24]. Therefore, ablating δ cells is likely to at least initially protect HFD mice from developing diabetes. Decreased SST secretion in HFD mice has also been established to lead to increased glucagon secretion[68], which may contribute to hyperglycemia but may also amplify insulin secretion above the β cell glucose threshold. Whether δ cells play a similar role in humans, who have a lower glycemic set point, is an important question to be resolved in subsequent studies. While removing δ cells from human islets would be challenging, it can potentially be achieved by sorting out δ cells

from dissociated islets by fluorescence-activated cell sorting using specific surface markers, then re-aggregating the islets without δ cells.

In summary, our findings illustrate that pancreatic δ cells determine the glycemic set point through their interaction with β cells. Our findings establish the physiological role of δ cells as local dampeners of insulin secretion during the resting state. Upon removal or inhibition of δ cells, we observe an immediate and sustained reduction of the glycemic set point. These observations are consistent with the increase in the glycemic set point known to occur around 2-3 weeks postnatally in mice[3,69] that we demonstrated is caused by onset of β cell UCN3 expression and subsequent increase of SST tone[24]. Our findings quantify the contribution of pancreatic δ cells and simultaneously indicate that their physiological role is to restrain β cells and moderate insulin secretion without preventing nutrient stimulation of β cell insulin secretion. In the absence of δ cells, β cell calcium responses and insulin secretion are intact but shifted to a new stable beta cell-autonomous set point. As such, δ cells are a prime example of the important and complementary role that paracrine feedback inhibition plays in determining important physiological parameters such as our glycemic set point. δ cell feedback accomplishes this in concert with the β cell autonomous glucose threshold, acting as redundant mechanisms that collectively safeguard against inappropriate and acutely dangerous hyperinsulinemic hypoglycemia.

METHODS

Animals

Mice were maintained on the C57BL/6 background in group housing (4 mice per cage) in a specific pathogen free facility on a 12 hr light:12 hr darkness cycle and an ambient temperature of 20-26°C, and humidity of 30-70%. Water and standard rodent chow were provided *ad libitum*. Heterozygous *Sst*-IRES-Cre mice (*Sst*$^{tm2.1(cre)Zjh}$/J, Jax #013044)[70] were crossed together to generate homozygous *Sst*-IRES-Cre mice (*Sst*-Cre$^{TG/TG}$). *Sst*-Cre$^{+/TG}$ x lsl-YFP (B6.129X1-*Gt(ROSA)26Sor*$^{tm1(EYFP)Cos}$/J, Jax # 006148)[71] mice were crossed to *Sst*-Cre$^{+/TG}$ to generate heterozygous and homozygous *Sst*-Cre x lsl-YFP mice. *Sst*-Cre x lsl-DTR mice were initially generated by crossing *Sst*-Cre$^{+/TG}$ mice to homozygous *R26-iDTR* mice (C57BL/6-*Gt(ROSA)26Sor*$^{tm1(HBEGF)Awai}$/J, Jax # 007900)[72], then maintained by crossing bi-transgenic offspring to C57BL/6N mice or by crossing mice with complementary transgenes. For tdTomato lineage-labeling, some of the mice were also crossed to *Ai14(RCL-tdT)-D* mice (B6.Cg-Gt(ROSA)26Sor$^{tm14(CAG-tdTomato)Hze/J}$, Jax # 007914)[73]. To ablate α cells, mice expressing *Gcg*-CreERT2 (B6;129S4-*Gcg*$^{em1(cre/ERT2)Khk}$/Mmjax, Jax #030346) [43] were also crossed to lsl-DTR mice. For β cell calcium imaging, *Sst*-Cre x lsl-DTR mice were crossed to mice expressing *MIP*-CreERT (B6.Cg-Tg(Ins1-cre/ERT)1Lphi/J, Jax # 024709)[74] and *Ai96(RCL-GCaMP6s)* (B6;129S6-*Gt(ROSA)26 Sor*$^{tm96(CAG-GCaMP6s)Hze}$/J, Jax # 24106)[75], then maintained by crossing mice expressing complementary transgenes, with one parent expressing lsl-DTR and the other expressing lsl-GCaMP6. *Sst*-Cre x lsl-Gi-DREADD mice were generated by crossing *Sst*-Cre$^{+/TG}$ mice to homozygous *R26-LSL-Gi-DREADD* mice (B6.129-Gt(ROSA)26 Sor$^{tm1(CAG-CHRM4*,-mCitrine)Ute}$/J, Jax # 026219)[76], then maintained by crossing bi-transgenic offspring to C57BL/6N mice or to complementary littermates.

Sst-Cre$^{TG/TG}$ mice were not used for breeding. Mice were used between 2 and 4 months of age unless otherwise indicated. We used animals of both sexes throughout our experimental design and reported the data separately by sex, except for the islet transplantation experiment in Fig. 5, which was performed with male donor and recipient mice only. All mouse experiments were approved by the UC Davis Institutional Animals Care and Use Committee and were performed in compliance with the Animal Welfare Act and the Institute for Laboratory Animal Research Guide to the Care and Use of Laboratory Animals.

Glucose measurements

Blood glucose levels were collected by tail prick followed by measurement using the OneTouch Ultra glucometer. Measurements were always performed in the afternoon between the hours of 3:00pm-5:00pm, and the order in which the mice were measured was kept consistent.

DT, tamoxifen, CNO, and streptozotocin treatments

For δ cell ablation, 126 ng diphtheria toxin (List Biological Laboratories, Catalog # 150) in 200 μL 0.9% saline was injected into mice via IP injection on days 0, 3, and 4. The same timeline for DT administration was followed for α cell ablation, except 300 ng was given. Control mice were given an intraperitoneal injection on the same days with an equivalent volume of 0.9% saline. Tamoxifen (Sigma-Aldrich, Catalog # T5648) was dissolved in sunflower oil (Trader Joe's, Monrovia, CA, USA) at 20 mg/mL, then administered to mice via oral gavage with a volume of 250 μL for 5 consecutive days. CNO (Tocris, Catalog # 4936) was dissolved in 0.9% saline and administered to mice at 1 mg/kg via IP injection. Streptozotocin (Calbiochem, now EMD Millipore, Catalog # 572201) was dissolved in 100 mM sodium citrate pH 4.5 and administered to mice at 50 mg/kg via IP injection for 5 consecutive days.

Glucose tolerance test and plasma insulin collection

Mice were fasted overnight for 16 hours. The next morning, they were weighed and put into individual cages. Tails were clipped with a surgical scissor and baseline glucose measured before administration of 2 mg/kg glucose via IP injection (Dextrose, Sigma-Aldritch, Catalog # D9559). *Sst*-Cre x Gi-DREADD mice were administered 1 mg/kg CNO via IP injection 1 hour before glucose. All blood glucose measurements over the 2-3 hour time period were done using a OneTouch Ultra glucometer. To collect plasma insulin, tail blood from mice was collected using the Microvette CB300 EDTA (Sarstedt, Catalog # 16.444.100) and kept on ice. After all the 15 min time points were collected, the samples were spun down at 4°C at 5000 rpm for 10 minutes and the plasma collected into a non-stick tube (Ambion, Catalog # AM12300). Samples were stored at −20°C until assayed.

Feeding measurements

Male *Sst*-Cre x lsl-DTR littermates were separated into single-housed cages and each given 100 g of chow. The amount of chow was measured by weight each day at the same time in the afternoon and subtracted from the previous day's amount of chow to determine the amount eaten.

Islet isolation

Islets were isolated by injecting 2 mL collagenaseP (0.8 mg/mL in HBSS, Roche Diagnostics, Catalog # 11249002001) into the bile duct with the ampulla of Vater clamped. The pancreas was removed into a conical tube to which an additional 2 mL of collagenaseP was added, then incubated at 37°C for 11 min. This was followed by gentle manual shaking to dissociate the pancreases, then three washes with cold HBSS + 5% NCS (Newborn Calf Serum). After the digested suspension was passed through a nylon mesh (pore size 425 μm, Small Parts), the islets were isolated by density gradient centrifugation using Histopaque (Sigma-Aldrich, Catalog # 10771) for 20 min at 1400 xg without brake. Islets were then collected from the interface, washed with cold HBSS + 5% NCS, and hand-picked several times under a dissecting microscope, followed by culture in RPMI + 5.5 mM Glucose + 10% FBS + pen/strep.

Static hormone secretion assays

Islets were picked twice into Krebs Ringer Buffer (20 mM Hepes pH 7.4, 1.2 mM KH_2PO_4, 25 mM $NaHCO_3$, 130 mM NaCl, 5 mM KCl, 1.2 mM $MgCl_2$, 1.2 mM $CaCl_2$) containing 0.1% BSA and 3 mM glucose (insulin secretion in Fig. 3 and glucagon secretion in Extended Fig. 4) or 5.5 mM glucose (SST and glucagon in Fig. 2 and Fig. 6, respectively), then incubated at 37°C for 1 hour. For insulin secretion, islets were pooled and split into different treatment groups with at least 5 replicates each and 10 islets per well, with different treatments added after the islets had been placed into the wells. Glucagon secretion was also measured from the same samples. For measurement of glucagon secretion in α cell-ablated islets, islets from each mouse were divided into two groups: one incubated in 5.5 mM glucose, and the other incubated in 5.5 mM glucose with the addition of 1 μM epinephrine, with at least 3 technical replicates per mouse and 40 islets per well. For SST secretion, islets were also pooled and then split into two treatment groups, 5.5 mM glucose or 5.5 mM glucose with 100 nM ghrelin, with at least 6 replicates each and 15 islets per well.

Calcium imaging and dynamic insulin secretion assays

We administered diphteria toxin to quadruple transgenic *MIP*-Cre/ERT x *Sst*-Cre x lsl-DTR x lsl-GCaMP6 mice on days 0, 3, and 4, followed after a 2-day pause by 5 days of tamoxifen administration to induce Cre-driven GCaMP6 expression in β cells. For imaging, microfluidics chambers were bonded to 35 mm dishes with a glass bottom (Mattek, Catalog # P35G-1.5-14-C). Islets were set down into these chambers and allowed to adhere to the glass by overnight culture. Continuous perfusion of Krebs Ringer Buffer at a rate of 200 μL per minute was maintained using the Elveflow microfluidics system, with different treatments adjusted using the Mux distributor. The calcium response of islets over time was imaged using a Nikon Eclipse Ti2 using a 60x lens with oil. Regions of interest (ROIs) were drawn around individual cells on NIS-Elements 5.02.01 and green fluorescence intensity in each ROI was measured to determine GCaMP6 activity over time. The half maximum intensity of each cell's calcium response was determined with a custom code written in Octave v6.2.0. Simultaneous collection of dynamic insulin perfusate was done by collecting the outflow into non-stick tubes.

Hormone measurements

Plasma insulin was measured using the Ultra-Sensitive Mouse Insulin ELISA Kit wide range assay (Crystal Chem, Catalog # 90080) and plasma glucagon was measured using the Glucagon ELISA kit (Mercodia, Catalog # 10-1281-01). Fold change in plasma insulin was calculated by dividing the plasma insulin levels of a mouse at 15 minutes divided by plasma insulin levels of the same mouse at 0 minutes. Secreted insulin was measured using the Lumit™ Insulin Immunoassay (Promega, Catalog # CS3037A01) in 384-well plates (Corning, Catalog # 3572) at 10 μL (static secretion) or 25 μL (dynamic secretion) sample volumes. Secreted glucagon was measured using the Lumit™ Glucagon Immunoassay (Promega, Catalog # W8022) in 384-well plates at 15 μL samples volumes. Secreted SST was measured using the Somatostatin EIA Kit (Phoenix Pharmaceuticals, Catalog # EK-060-03).

Immunofluorescence

Pancreases were isolated with the spleen and fixed in 4% PFA for 5 hours, then protected with 30% sucrose overnight prior to embedding with OCT (Fisher Healthcare, Catalog # 4585). Cryosections of 14 μm thickness were collected using a Leica cryostat. The same procedure was conducted with the stomach, which was isolated, halved lengthwise, and washed twice in PBS prior to fixation in PFA, and the duodenum, which was collected as an approximately 1 cm piece adjacent to the stomach and opened up prior to fixation. The brain was fixed in 4% borate PFA for 24 hours, protected with 30% sucrose overnight, and collected as 50 μm thick sections using a vibratome. For immunofluorescence, slides were first washed for 5 minutes three times in KBS, then incubated with antibodies diluted in donkey block (KPBS supplemented with 2% donkey serum and 0.4% Triton X-100) overnight at 4°C. Tissue samples were incubated with secondary antibodies diluted in donkey block the following day and mounted using ProLong Gold Antifade Mountant (Invitrogen, Catalog # P36930). Slides were imaged on a Nikon Eclipse Ti using a 60x lens with oil. For whole mount staining of islets after calcium imaging, islets were fixed in 4% PFA in the chamber for 15 minutes at room temperature, then washed in PBS twice before a 15-minute incubation at 4°C. Islets were incubated in donkey block overnight at 4°C, followed by overnight incubation with primary antibodies diluted in donkey block, overnight wash in PBS + 0.15% Tween 20, and overnight incubation with secondary antibodies diluted in donkey block. Finally, islets were incubated in 4% PFA either overnight at 4°C or for 1 hour at room temperature, followed by several washes in PBS + 0.15% Tween 20 every 30 minutes. After the washes, the islets were put in Rapiclear (SunJin Lab, Catalog # RC152001) and imaged on a Nikon Eclipse Ti2.

Antibodies

Primary antibodies used were guinea pig polyclonal anti-insulin (Dako Catalog # A0564; 1:500), rat monoclonal anti-insulin (R&D Systems Catalog # MAB1417, Clone # 182410; 1:500), rabbit polyclonal anti-glucagon (Cell Signaling Technology Catalog # 2760S; 1:400), guinea pig polyclonal anti-glucagon (Progen Catalog # 16032; 1:1000), sheep polyclonal anti-somatostatin (American Research Products Catalog # 13-2366; 1:1000), rat monoclonal anti-somatostatin (Abcam Catalog # AB30788; Clone # M09204, 1:300),

rabbit polyclonal anti-Urocortin 3 (gift from Wylie Vale, #7218; 1:1000), and goat polyclonal anti-GFP (Rockland Catalog # 600-101-215; 1:1000). Secondary antibodies used were DyLight 405-AffiniPure Donkey Anti-Guinea Pig IgG (H+L) (Jackson ImmunoResearch #706-475-148), Cy3-AffiniPure F(ab')2 Fragment Donkey Anti-Guinea Pig IgG (H+L) (Jackson ImmunoResearch #706-166-148), 647-AffiniPure F(ab')$_2$ Fragment Donkey Anti-Guinea Pig IgG (H+L) (Jackson ImmunoResearch #706-606-148), Cy3-AffiniPure F(ab')2 Fragment Donkey Anti-Rat IgG (H+L) (Jackson ImmunoResearch #712-166-153), 647-AffiniPure F(ab')2 Fragment Donkey Anti-Rat IgG (H+L) (Jackson ImmunoResearch #712-606-153), 488-AffiniPure Goat Anti-Mouse IgG, F(ab')2 Fragment (Jackson ImmunoResearch #115-545-072), DyLight 488-AffiniPure F(ab')2 Fragment Donkey Anti-Sheep IgG (Jackson ImmunoResearch #713-486-147), Cy3-AffiniPure F(ab')2 Fragment Donkey Anti-Rabbit IgG (H+L) (Jackson ImmunoResearch #711-166-152), 647-AffiniPure Donkey Anti-Rabbit IgG (H+L) (Jackson ImmunoResearch #711-605-152). All secondary antibodies were used at a 1:600 dilution.

Cell quantification

Islet cells were counted manually using FIJI 2.9.0 and the CellCounter plugin. At least 500 cells across 10 islets were counted per mouse. Quantification of *Sst*-Cre driven tdTomato+ neurons within the brain was conducted via a semi-automated algorithm written in Python 3.9 and implemented in napari 0.4.16 [77]. Regions of Interest (ROIs) of tdTomato+ neurons were made using the protocol outlined in Postić et al., 2023 [78]. First, two blurred images were produced using gaussian blur with the second blurred image produced using a kernel twice the size of the first. These blurred images were then subtracted from one another, effectively creating a bandpass-filtered image highlighting circular features roughly the size of a single SST+ neuron cell body in our image. Local maxima within the bandpass-filtered image were used to define the center of each neuron. To define pixels residing within neurons, a small positive threshold was applied to the bandpass-filtered image. These pixels were then assigned to their nearest local maxima to create a mask. Each image was then displayed in napari with the generated mask superimposed. We manually reviewed the ROIs in each image and erased ROIs created by the bright edge of the brain slice, an artifact of imaging. The mask was then updated and the number of ROIs within the mask was quantified and tabulated. To quantify specific regions of the brain, a shape layer of the corresponding region (cortex or hypothalamus) was manually drawn for each brain. This shape layer was then used as a mask to isolate and then tabulate ROIs within these defined regions of the brain.

RNA Extraction and qPCR

Tissues were collected into TRIzol Reagent (Invitrogen, Catalog # 15596026). Prior to the start of the RNA extraction, hypothalamus, stomach, and duodenal tissue collected into TRIzol were sonicated. Islets were directly broken down in TRIzol. RNA was isolated by chloroform extraction and precipitated by isopropanol. Once pellets were resuspended, cDNA was made using a High-Capacity cDNA Reverse Transcription Kit (Applied Biosystems, Catalog # 4368813). qPCR was performed using the PowerUp SYBR Green Master Mix (Applied Biosystems, Catalog # A25741) or iTaq Universal SYBR Green Supermix (Bio-Rad, Catalog # 1725121) on a Bio-Rad CFX 384. Primers

were designed using the Roche Universal Probe Library online design tool. *Ins2* (RefSeq NM_001185084): forward primer – 5' GCTCTCTACCTGGTGTGTGGG 3'; reverse primer – 5' CAAGGTCTGAAGGTCACCTGC 3'; expected amplicon: 128 bp. *Gcg* (RefSeq NM_008100): forward primer – 5' TCACAGGGCACATTCACCAG 3'; reverse primer – 5' CATCATGACGTTTGGCAATGTT 3'; expected amplicon: 121 bp. *Sst* (RefSeq NM_009215): forward primer – 5' GACCCCAGACTCCGTCAGTTT 3'; reverse primer – 5' TCTCTGTCTGGTTGGGCTCG 3'; expected amplicon: 112 bp.

Continuous glucose monitoring

Mice were anesthetized, shaved, and sterilized. A Dexcom G6 sensor was introduced subcutaneously into mice and bonded using veterinary glue. Receivers were left adjacent to cages and monitored. Continuous Glucose Monitoring profiles were collected for approximately a week.

Islet transplant under the kidney capsule

Islets from male *Sst*-Cre$^{+/TG}$ x lsl-DTR mice and *Sst*-Cre$^{+/TG}$ controls were cultured overnight in RPMI + 10% FBS + pen/strep + 5.5 mM glucose, then collected into an eppendorf tube and allowed to settle. Recipients were male STZ-induced age-matched wild-type mice (without the *Sst*-Cre nor lsl-DTR transgenes) born from the same litter as the donors. Stable hyperglycemia was determined as at least three consecutive glucose measurements of >300 mg/dL. Islet transplant into the kidney capsule was performed based on another paper (Szot et al. 2007)[79]. Following anaesthetization with isoflurane, mice were shaved on the left flank and an incision was made to provide access to the left kidney. The left kidney was lifted from the retroperitoneal cavity and a small scratch was made to allow for the insertion of the beveled tip of PE10 tubing attached to a p200 pipette. One hundred islets pre-loaded into the tubing were advanced out by the dial of the pipette and the tubing carefully retracted after all the islets had entered the capsule. The scratch on the kidney was closed by cauterization and the mouse was sutured after placing the kidney back into the retroperitoneal cavity. After normoglycemia was re-established in the recipients, DT was administered at the same dose and regimen as described above - 126 ng DT in 200 μL 0.9% saline was administered via IP injection, then administered two more times 3 and 4 days after the initial injection.

Statistical analysis

Glucose measurements and body weight were analyzed by two-way ANOVA with repeated measures for effect of genotype/treatment (DT-mediated ablation or CNO), followed by Holm-Sidak's multiple comparison test. GTTs, glucose-stimulated plasma insulin measurements, and secretion assays were analyzed by two-way ANOVA with repeated measures for effect of genotype/treatment and interaction between genotype/treatment and glucose followed by Holm-Sidak's multiple comparison test. AUC-Baseline data were analyzed by two-tailed unpaired t-test. Cell quantifications were analyzed by two-tailed unpaired t-test or by one-way ANOVA followed by Holm-Sidak's multiple comparison test where appropriate. CGM data was analyzed by averaging glucose levels of the mice at each time point and then one-way ANOVA followed by Holm-Sidak's multiple comparison test. Octave 6.2.0 was used to write the code to determine the half-maximum as the activity

threshold at which each β cell first responds. These data were plotted in a Kaplan-Meier curve and analyzed with the Mantel-Cox test. All line and bar graphs are represented as mean ± SEM unless stated otherwise, with n representing number of animals in each group. Data points connected by lines over time represent repeated measurement on the same animals. All statistical tests performed were two-sided and differences were considered significant when $p < 0.05$. Statistics were computed using Prism 8 (GraphPad Software, La Jolla, CA).

Extended Data

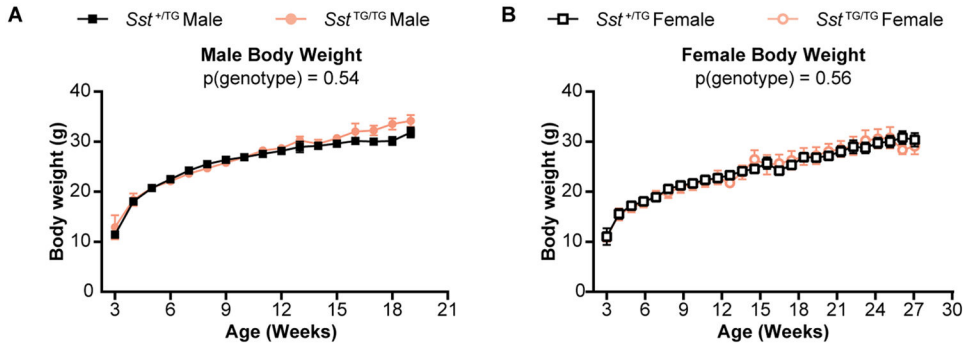

Extended Figure 1:

A) Body weight measurements of male *Sst*-Cre$^{+/TG}$ and *Sst*-Cre$^{TG/TG}$ mice from Fig. 1D (n=6 *Sst*-Cre$^{+/TG}$, n=9 *Sst*-Cre$^{TG/TG}$). B) Body weight measurements of female *Sst*-Cre$^{+/TG}$ and *Sst*-Cre$^{TG/TG}$ mice from Fig. 1E (n=7 *Sst*-Cre$^{+/TG}$, n=7 *Sst*-Cre$^{TG/TG}$). Significance was determined by two-way ANOVA or mixed modeling for genotype and age followed by Holm-Sidak's correction for multiple comparisons. Error bars represent SEM.

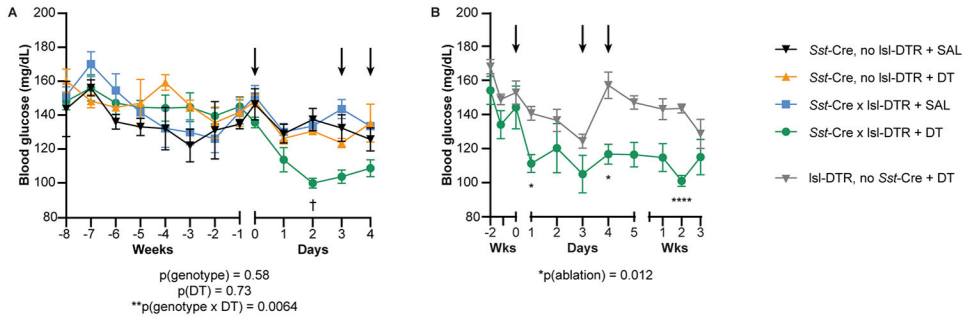

Extended Figure 2:

A) Blood glucose measurements of SAL and DT-treated male *Sst*-Cre only (n=3 and n=4, respectively) and SAL and DT-treated *Sst*-Cre x lsl-DTR (n=5 and n=6, respectively) male mice. Black arrows represent IP administration of DT. Significance was determined by three-way ANOVA for genotype and DT administration, followed by multiple comparisons of every mean to every other mean and Holm-Sidak's correction. Error bars represent SEM. † represents statistically significant difference (p=0.029) between DT-treated *Sst*-Cre only and *Sst*-Cre x lsl-DTR mice. B) Blood glucose measurements of male DT-treated lsl-DTR only (n=6) and *Sst*-Cre x lsl-DTR (n=5) mice. Black arrows represent IP administration

of DT. Significance was determined by two-way ANOVA for ablation followed by Holm-Sidak's correction for multiple comparisons (A; B, *p=0.022, *p=0.022, ****p<0.0001). Error bars represent SEM.

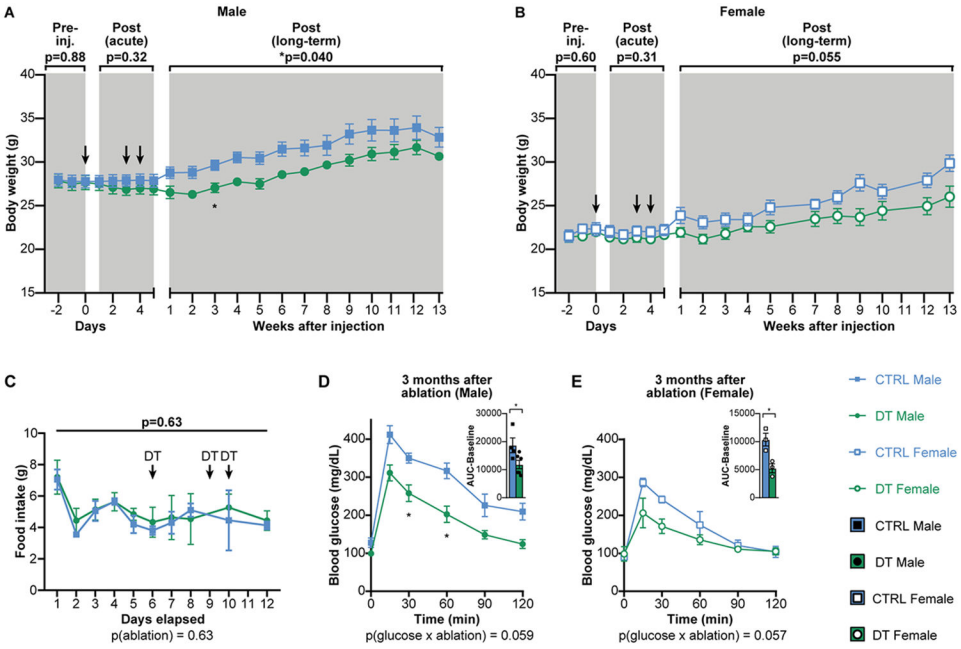

Extended Figure 3:

A) Body weight measurements of male CTRL and DT mice in Fig. 3A (n=8 CTRL, n=6 DT). Black arrows represent IP administration of SAL or DT. B) Body weight measurements of female CTRL and DT mice in Fig. 3B (n=6 CTRL, n=6 DT). Black arrows represent IP administration of SAL or DT. C) Feeding measurements in DT-treated *Sst*-Cre x lsl-DTR (n=3) and *Sst-Cre* only (n=3) mice. Black arrows represent IP administration of DT. D) Glucose tolerance test of male mice 3 months after ablation (n=4 CTRL, n=6 DT). E) Glucose tolerance test of female mice 3 months after ablation (n=3 CTRL, n=3 DT). Significance was determined by two-way ANOVA for ablation (A, B, C) or ablation and glucose (D, E) followed by Holm-Sidak's correction for multiple comparisons (A: *p=0.039; D: *p=0.045, *p=0.032) or two-tailed unpaired t-test (AUC-Baseline for D, *p=0.040; AUC-Baseline for E, *p=0.021). Error bars represent SEM.

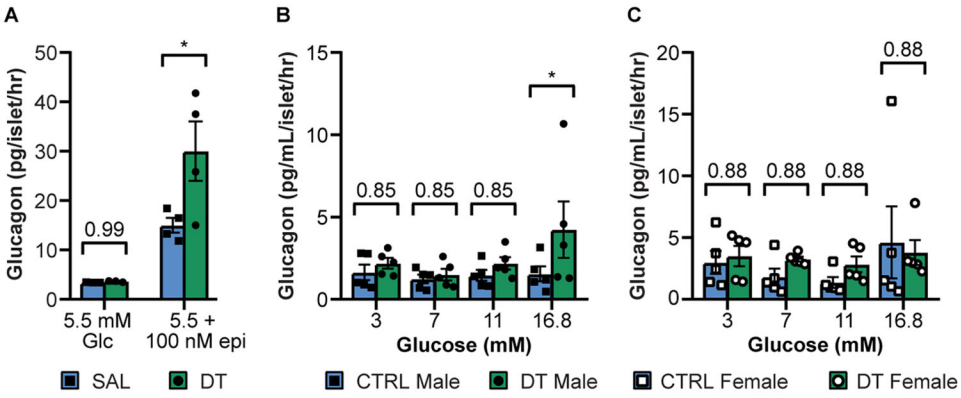

Extended Figure 4:

A) Static glucagon secretion assay performed on islets isolated from SAL- or DT-treated *Sst*-Cre x lsl-DTR mice (n=4 each). Islets were stimulated with 100 nM epinephrine to stimulate glucagon secretion. B) Static glucagon secretion assay performed on the same islets from Figure 3M (n=5 replicates per group, 10 islets each, pooled from 3 CTRL or 3 DT mice). C) Static glucagon secretion performed on the same islets from Figure 3N (n=5 replicates per group, 10 islets each, pooled from 3 CTRL or 3 DT mice). Significance was determined by two-way ANOVA followed by Holm-Sidak's correction for multiple comparisons (A, *p=0.015; B, *p=0.042; C). Error bars represent SEM.

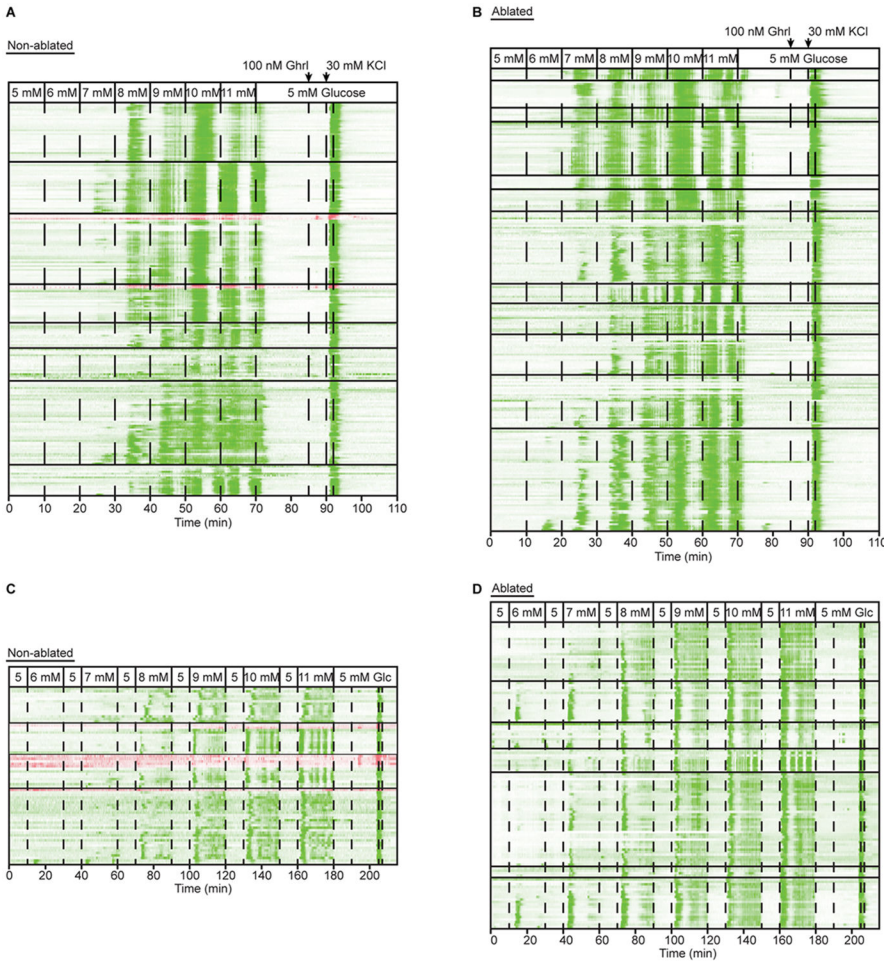

Extended Figure 5:

A) Non-ablated and B) ablated islet calcium responses. Each box represents an islet. Each line represents calcium activity of a single β (green) or δ (red) cell. Dashed lines represent points at which glucose levels were changed. Ghrelin was used to functionally distinguish δ cells. 30 mM KCl was used to confirm viability of the cells. C and D) Traces from the same C) non-ablated and D) ablated mice in which islets were perfused with 5 mM glucose between each glucose step to confirm that the responses are not due to time or a delayed response to previous glucose levels.

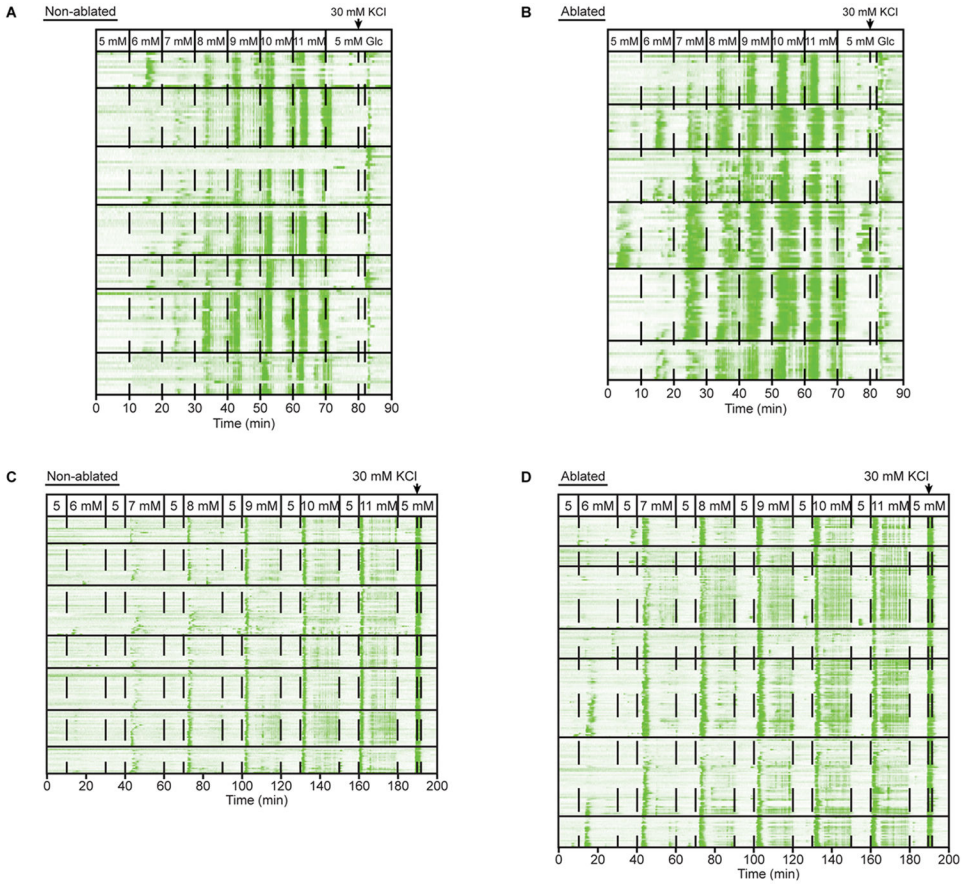

Extended Figure 6:

A) Non-ablated and B) ablated islet calcium responses. Each box represents an islet. Each line represents calcium activity of a single β cell. Dashed lines represent points at which glucose levels were changed. 30 mM KCl was used to confirm viability of the cells. C and D) Traces from the same C) non-ablated and D) ablated mice in which islets were perfused with 5 mM glucose between each glucose step to confirm that the responses are not due to time or a delayed response to previous glucose levels. 30 mM KCl was used to confirm viability of the cells.

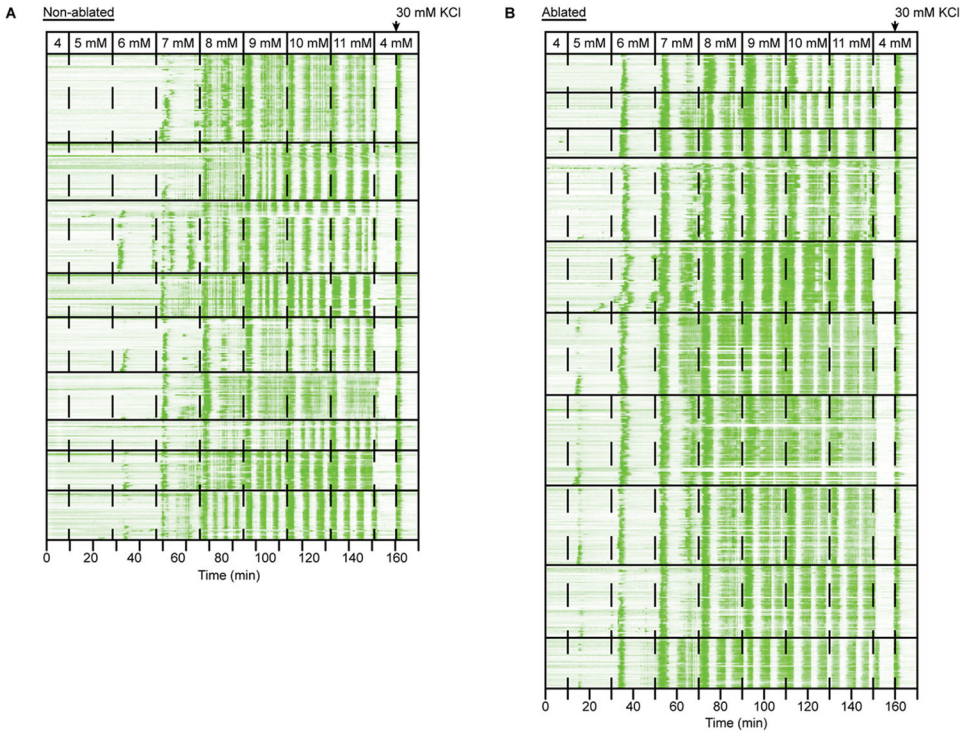

Extended Figure 7:

A) Non-ablated and B) ablated islet calcium responses. Each box represents an islet. Each line represents calcium activity of a single β cell. Dashed lines represent points at which glucose levels were changed. 30 mM KCl was used to confirm viability of the cells.

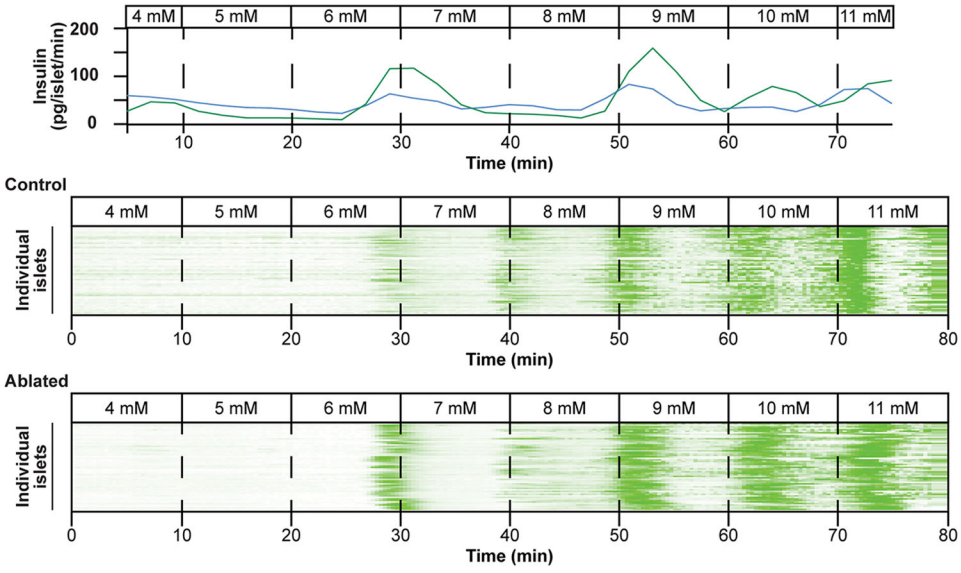

Extended Figure 8:

The top graph shows insulin secretion over time from control (blue) and δ cell-ablated (green) islets as glucose is raised from 4 mM to 11 mM glucose. Below are the respective

calcium traces of whole islets (n = 60 each) from the control (middle) and δ cell-ablated (bottom) mouse imaged at 4x. Each row represents the response of an individual islet.

Supplementary Material

Refer to Web version on PubMed Central for supplementary material.

ACKNOWLEDGEMENTS

This work was supported by the National Institute of Diabetes and Digestive and Kidney Disease (NIDDK-110276; MOH). J.L.H was supported by a National Institute of General Medical Sciences-funded Pharmacology Training Program (T32 GM-099608). S.L. was supported by the NSF Graduate Research Fellowship (1650042), the UC Davis Training Program in Molecular and Cellular Biology (T32 GM-007377), and the UC Davis NSF Bridge to Doctorate Program (1612490). M.S.P. is supported by the UC Davis Training Program in Molecular and Cellular Biology (T32 GM-007377).

DATA AVAILABILITY

All data generated or analyzed during this study are included in this published article and its supplementary information files. Source data are available with this paper. Data for relevant images have made available at Figshare: https://doi.org/10.6084/m9.figshare.24082434 [80]

CODE AVAILABILITY

The code used to perform glucose threshold analysis and neuron quantification is available on GitHub: https://github.com/Huising-Lab/Paracrine-signaling-by-pancreatic-mouse-cells-determines-the-glycemic-set-point.

REFERENCES

1. Matschinsky FM & Davis EA The Distinction between ‘Glucose Setpoint’, ‘Glucose Threshold’ and ‘Glucose Sensor’ is Critical for Understanding the Role of the Pancreatic β-Cell in Glucose Homeostasis. Mol. Cell Biol. Type 2 Diabetes Its Complicat 14, 14–29 (1998).
2. Gerich JE Control of glycaemia. Bailliere’s Clinical Endocrinology and Metabolism vol. 7 (1993).
3. Blum B. et al. Functional beta-cell maturation is marked by an increased glucose threshold and by expression of urocortin 3. Nat. Biotechnol 30, 261–264 (2012). [PubMed: 22371083]
4. Rodriguez-Diaz R. et al. Paracrine Interactions within the Pancreatic Islet Determine the Glycemic Set Point. Cell Metab. 27, 549–558.e4 (2018). [PubMed: 29514065]
5. Ewing KL & Tauber OE Blood chemistry changes in mice fed high levels of polyoxyethylene sorbitan derivatives. Toxicol. Appl. Pharmacol 6, 442–446 (1964). [PubMed: 14223494]
6. Chambers AP et al. The Role of Pancreatic Preproglucagon in Glucose Homeostasis in Mice. Cell Metab. 25, 927–934.e3 (2017). [PubMed: 28325479]
7. Svendsen B. et al. Insulin Secretion Depends on Intra-islet Glucagon Signaling. Cell Rep. 25, 1127–1134.e2 (2018). [PubMed: 30380405]
8. Capozzi ME et al. Glucagon lowers glycemia when β cells are active. JCI Insight 4, (2019).
9. Zhu L. et al. Intraislet glucagon signaling is critical for maintaining glucose homeostasis. JCI Insight 4, (2019).
10. Tellez K. et al. In vivo studies of glucagon secretion by human islets transplanted in mice. Nat. Metab 2, 547–557 (2020). [PubMed: 32694729]
11. Capozzi ME et al. β Cell tone is defined by proglucagon peptides through cAMP signaling. JCI insight 4, (2019).

12. Liu L. et al. Gq signaling in α cells is critical for maintaining euglycemia. JCI Insight 6, 1–17 (2021).
13. Huising MO Paracrine regulation of insulin secretion. Diabetologia 63, 2057–2063 (2020). [PubMed: 32894316]
14. Pagliara AS, Stillings SN, Hover B, Martin DM & Matschinsky FM Glucose modulation of amino acid induced glucagon and insulin release in the isolated perfused rat pancreas. J. Clin. Invest 54, 819–832 (1974). [PubMed: 4430716]
15. Alonge KM, D'Alessio DA & Schwartz MW Brain control of blood glucose levels: implications for the pathogenesis of type 2 diabetes. Diabetologia 64, 5–14 (2021). [PubMed: 33043401]
16. Cheng W. et al. Hindbrain circuits in the control of eating behaviour and energy balance. Nat. Metab 4, 826–835 (2022). [PubMed: 35879458]
17. Thorens B. Sensing of glucose in the brain. Handb. Exp. Pharmacol 209, 277–294 (2012).
18. German JP et al. Leptin activates a novel CNS mechanism for insulin-independent normalization of severe diabetic hyperglycemia. Endocrinology 152, 394–404 (2011). [PubMed: 21159853]
19. Ryan KK et al. Fibroblast growth factor-19 action in the brain reduces food intake and body weight and improves glucose tolerance in male rats. Endocrinology 154, 9–15 (2013). [PubMed: 23183168]
20. Morton GJ et al. FGF19 action in the brain induces insulin-independent glucose lowering. J. Clin. Invest 123, 4799–4808 (2013). [PubMed: 24084738]
21. Carroll PB, Zeng Y, Alejandro R, Starzl TE & Ricordi C Glucose homeostasis is regulated by donor islets in xenografts. Transplant. Proc 24, 2980–2981 (1992). [PubMed: 1466022]
22. Vieira E, Salehi A & Gylfe E Glucose inhibits glucagon secretion by a direct effect on mouse pancreatic alpha cells. Diabetologia 50, 370–379 (2007). [PubMed: 17136393]
23. Lai BK et al. Somatostatin is only partly required for the glucagonostatic effect of glucose but is necessary for the glucagonostatic effect of KATP channel blockers. in Diabetes vol. 67 2239–2253 (2018). [PubMed: 30115649]
24. van der Meulen T. et al. Urocortin3 mediates somatostatin-dependent negative feedback control of insulin secretion. Nat. Med 21, 769–76 (2015). [PubMed: 26076035]
25. Shuai H, Xu Y, Yu Q, Gylfe E & Tengholm A Fluorescent protein vectors for pancreatic islet cell identification in live-cell imaging. Pflugers Arch. Eur. J. Physiol 468, 1765–1777 (2016). [PubMed: 27539300]
26. Xu SFS, Andersen DB, Izarzugaza JMG, Kuhre RE & Holst JJ In the rat pancreas, somatostatin tonically inhibits glucagon secretion and is required for glucose-induced inhibition of glucagon secretion. Acta Physiol. (2020) doi:10.1111/apha.13464.
27. Mandarino L, Stenner D, Blanchard W, Nissen S & Gerich J Selective effects of somatostatin-14, −25 and −28 on in vitro insulin and glucagon secretion. Nature 291, 76–77 (1981). [PubMed: 6112710]
28. Strowski MZ, Parmar RM, Blake AD & Schaeffer JM Somatostatin Inhibits Insulin and Glucagon Secretion via Two Receptor Subtypes: An in Vitro Study of Pancreatic Islets from Somatostatin Receptor 2 Knockout Mice. Endocrinology 141, 111–117 (2000). [PubMed: 10614629]
29. Hauge-Evans AC et al. Somatostatin secreted by islet δ-cells fulfills multiple roles as a paracrine regulator of islet function. Diabetes 58, 403–411 (2009). [PubMed: 18984743]
30. Singh B. et al. KATP channel blockers control glucagon secretion by distinct mechanisms: A direct stimulation of α-cells involving a [Ca2+]c rise and an indirect inhibition mediated by somatostatin. Mol. Metab 53, 101268 (2021). [PubMed: 34118477]
31. van der Meulen T. et al. Urocortin 3 Marks Mature Human Primary and Embryonic Stem Cell-Derived Pancreatic Alpha and Beta Cells. PLoS One 7, 1–12 (2012).
32. Blum B. et al. Reversal of β cell de-differentiation by a small molecule inhibitor of the TGFβ pathway. Elife 3, e02809 (2014). [PubMed: 25233132]
33. Kavalakatt S. et al. Urocortin 3 Levels Are Impaired in Overweight Humans With and Without Type 2 Diabetes and Modulated by Exercise. Front. Endocrinol. (Lausanne) 10, 1–11 (2019). [PubMed: 30723457]

34. Huising MO, van der Meulen T, Huang JL, Pourhosseinzadeh MS & Noguchi GM The Difference δ-Cells Make in Glucose Control. Physiology 33, 403–411 (2018). [PubMed: 30303773]
35. Thorel F. et al. Normal glucagon signaling and β-cell function after near-total α-cell ablation in adult mice. Diabetes 60, 2872–2882 (2011). [PubMed: 21926270]
36. Pedersen J. et al. Glucose metabolism is altered after loss of L cells and α-cells but not influenced by loss of K cells. Am. J. Physiol. - Endocrinol. Metab 304, 60–73 (2013).
37. Shiota C. et al. α-cells are dispensable in postnatal morphogenesis and maturation of mouse pancreatic islets. Am. J. Physiol. - Endocrinol. Metab 305, 1030–1040 (2013).
38. Viollet C. et al. Somatostatin-IRES-cre mice: Between knockout and wild-type? Front. Endocrinol. (Lausanne) 8, 1–8 (2017). [PubMed: 28144230]
39. Arrojo e Drigo R. et al. Structural basis for delta cell paracrine regulation in pancreatic islets. Nat. Commun 10, 3700 (2019). [PubMed: 31420552]
40. Barker N. Adult intestinal stem cells: Critical drivers of epithelial homeostasis and regeneration. Nat. Rev. Mol. Cell Biol 15, 19–33 (2014). [PubMed: 24326621]
41. Luo SX et al. Regulation of feeding by somatostatin neurons in the tuberal nucleus. Science (80-.). 361, 76–81 (2018).
42. Chen YC et al. Elevated islet prohormone ratios as indicators of insulin dependency in auto-islet transplant recipients. Am. J. Transplant 22, 1992–2005 (2022). [PubMed: 35506189]
43. Ackermann AM, Zhang J, Heller A, Briker A & Kaestner KH High-fidelity Glucagon-CreER mouse line generated by CRISPR-Cas9 assisted gene targeting. Mol. Metab 6, 236–244 (2016).
44. Brazeau P. et al. Hypothalamic polypeptide that inhibits the secretion of immunoreactive pituitary growth hormone. Science (80-.) 179, 77–79 (1973).
45. Dubois MP Immunoreactive somatostatin is present in discrete cells of the endocrine pancreas. Proc. Natl. Acad. Sci. U. S. A 72, 1340–1343 (1975). [PubMed: 1093177]
46. Koerker DJ et al. Somatostatin: Hypothalamic inhibitor of the endocrine pancreas. Science (80-.) 184, 482–484 (1974).
47. De Paoli M, Zakharia A & Werstuck GH The Role of Estrogen in Insulin Resistance: A Review of Clinical and Preclinical Data. Am. J. Pathol 191, 1490–1498 (2021). [PubMed: 34102108]
48. Hevener AL, Zhou Z, Moore TM, Drew BG & Ribas V The impact of ERα action on muscle metabolism and insulin sensitivity – Strong enough for a man, made for a woman. Mol. Metab 15, 20–34 (2018). [PubMed: 30005878]
49. Richardson CC et al. Increased perinatal remodelling of the pancreas in somatostatin-deficient mice: Potential role of transforming growth factor-beta signalling in regulating beta cell growth in early life. Horm. Metab. Res 47, 56–63 (2015). [PubMed: 25350519]
50. Luque RM & Kineman RD Gender-Dependent Role of Endogenous Somatostatin in Regulating Growth Hormone-Axis Function in Mice. 148, 5998–6006 (2007).
51. Luque RM, Cordoba-chacon J & Pozo-salas AI Obesity- and gender-dependent role of endogenous somatostatin and cortistatin in the regulation of endocrine and metabolic homeostasis in mice. Nat. Publ. Gr 1–12 (2016) doi:10.1038/srep37992.
52. Gahete MD et al. Cortistatin Is Not a Somatostatin Analogue but Stimulates Prolactin Release and Inhibits GH and ACTH in a Gender-Dependent Fashion : Potential Role of Ghrelin. 152, 4800–4812 (2011). [PubMed: 21971153]
53. Zaborska KE et al. Liraglutide increases islet Ca2+ oscillation frequency and insulin secretion by activating hyperpolarization-activated cyclic nucleotide-gated channels. Diabetes, Obes. Metab 1–12 (2022) doi:10.1111/dom.14747.
54. Bloom SR et al. Inhibition of Gastrin and Gastric-Acid Secretion By Growth-Hormone Release-Inhibiting Hormone. Lancet 304, 1106–1109 (1974).
55. Holst JJ, Orskov C & Seier-Poulsen S Somatostatin is an essential paracrine link in acid inhibition of gastrin secretion. Digestion 51, 95–102 (1992). [PubMed: 1354190]
56. Johansson C, Wisen O, Efendic S & Uvnäs-Wallensten K Effects of Somatostatin on Gastrointestinal Propagation and Absorption of Oral Glucose in Man. Digestion 22, 126–137 (1981). [PubMed: 6116637]

57. Holst JJ, Gribble F, Horowitz M & Rayner CK Roles of the gut in glucose homeostasis. Diabetes Care 39, 884–892 (2016). [PubMed: 27222546]
58. Karasawa H. et al. Brain somatostatin receptor 2 mediates the dipsogenic effect of central somatostatin and cortistatin in rats: Role in drinking behavior. Am. J. Physiol. - Regul. Integr. Comp. Physiol 307, R793–R801 (2014). [PubMed: 25031229]
59. Stengel A & Taché Y Central somatostatin signaling and regulation of food intake. Ann. N. Y. Acad. Sci 1455, 98–104 (2019). [PubMed: 31237362]
60. Huang C. et al. Depleting hypothalamic somatostatinergic neurons recapitulates diabetic phenotypes in mouse brain, bone marrow, adipose and retina. Diabetologia 64, 2575–2588 (2021). [PubMed: 34430981]
61. Li N. et al. Ablation of somatostatin cells leads to impaired pancreatic islet function and neonatal death in rodents article. Cell Death Dis. 9, (2018).
62. Ivanova A. et al. In vivo genetic ablation by Cre-mediated expression of diphtheria toxin fragment A. Genesis 43, 129–135 (2005). [PubMed: 16267821]
63. Zhang J, Mckenna LB, Bogue CW & Kaestner KH The diabetes gene Hhex maintains δ -cell differentiation and islet function. Genes Dev. 829–834 (2014) doi:10.1101/gad.235499.113. [PubMed: 24736842]
64. Noguchi GM & Huising MO Integrating the inputs that shape pancreatic islet hormone release. Nature Metabolism vol. 1 1189–1201 (2019).
65. Caicedo A. Paracrine and autocrine interactions in the human islet: More than meets the eye. Semin. Cell Dev. Biol 24, 11–21 (2013). [PubMed: 23022232]
66. Steiner DJ, Kim A, Miller K & Hara M Pancreatic islet plasticity: Interspecies comparison of islet architecture and composition. Islets 2, 135–145 (2010). [PubMed: 20657742]
67. Walker JT, Saunders Di. C., Brissova M & Powers AC The Human Islet: Mini-Organ with Mega-Impact. Endocr. Rev 42, 605–657 (2021). [PubMed: 33844836]
68. Kellard JA et al. Reduced somatostatin signalling leads to hypersecretion of glucagon in mice fed a high-fat diet. Mol. Metab 40, 101021 (2020). [PubMed: 32446876]
69. Rozzo A, Meneghel-Rozzo T, Delakorda SL, Yang SB & Rupnik M Exocytosis of insulin: In vivo maturation of mouse endocrine pancreas. in Annals of the New York Academy of Sciences vol. 1152 53–62 (2009). [PubMed: 19161376]
70. Taniguchi H. et al. A Resource of Cre Driver Lines for Genetic Targeting of GABAergic Neurons in Cerebral Cortex. Neuron 71, 995–1013 (2011). [PubMed: 21943598]
71. Srinivas S. et al. Cre reporter strains produced by targeted insertion of EYFP and ECFP into the ROSA26 locus. BMC Dev. Biol 1, 1–8 (2001). [PubMed: 11178105]
72. Buch T. et al. A Cre-inducible diphtheria toxin receptor mediates cell lineage ablation after toxin administration. Nat. Methods 2, 419–426 (2005). [PubMed: 15908920]
73. Madisen L. et al. A robust and high-throughput Cre reporting and characterization system for the whole mouse brain. Nat. Neurosci 13, 133–140 (2010). [PubMed: 20023653]
74. Wicksteed B. et al. Conditional gene targeting in mouse pancreatic β-cells: Analysis of ectopic cre transgene expression in the brain. Diabetes 59, 3090–3098 (2010). [PubMed: 20802254]
75. Madisen L. et al. Transgenic mice for intersectional targeting of neural sensors and effectors with high specificity and performance. Neuron 85, 942–958 (2015). [PubMed: 25741722]
76. Zhu H. et al. Cre-dependent DREADD (Designer Receptors Exclusively Activated by Designer Drugs) mice. Genesis 54, 439–446 (2016). [PubMed: 27194399]
77. Sofroniew N. et al. napari: a multi-dimensional image viewer for Python. (2022) doi:10.5281/ZENODO.7276432.
78. Postić S. et al. High-resolution analysis of the cytosolic Ca2+ events in β cell collectives in situ. Am. J. Physiol. Endocrinol. Metab 324, E42–E55 (2023). [PubMed: 36449570]
79. Szot GL, Koudria P & Bluestone JA Transplantation of pancreatic islets into the kidney capsule of diabetic mice. J. Vis. Exp 9–10 (2007) doi:10.3791/404.
80. Huang JL, Pourhosseinzadeh MS & Huising MO Paracrine signaling by pancreatic mouse δ cells determines the glycemic set point. figshare. Dataset (2023) doi:10.6084/m9.figshare.24082434.

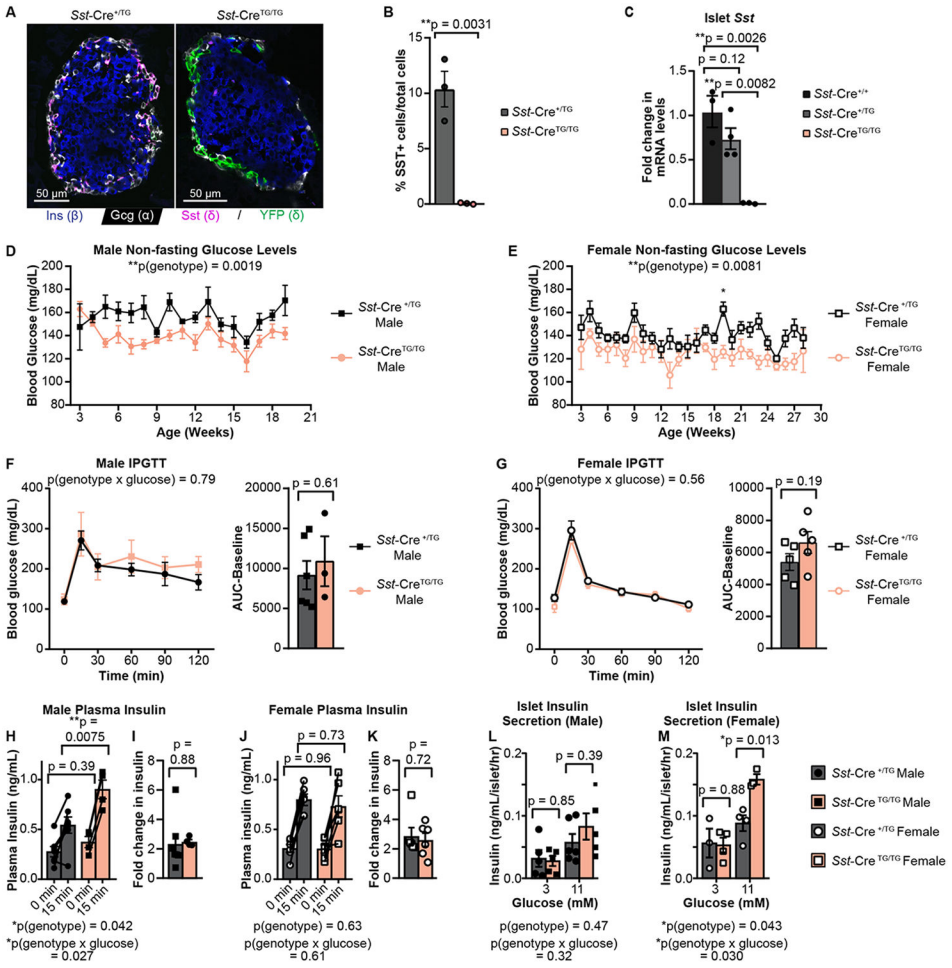

Fig. 1. *Sst*-Cre$^{TG/TG}$ mice exhibit loss of *Sst* and a decreased glycemic set point.

A) Immunofluorescent stain of pancreas section from a *Sst*-Cre$^{+/TG}$ x lsl-YFP (left) and *Sst*-Cre$^{TG/TG}$ x lsl-YFP mouse (right). B) Quantification of SST+ cell number (n=3 *Sst*-Cre$^{+/TG}$, n=3 *Sst*-Cre$^{TG/TG}$). C) *Sst* mRNA levels in islets from *Sst*-Cre$^{+/+}$ (n=3), *Sst*-Cre$^{+/TG}$ (n=4), and *Sst*-Cre$^{TG/TG}$ (n=3) mice. D and E) Weekly blood glucose measurements of male (D, n=6 *Sst*-Cre$^{+/TG}$, n=9 *Sst*-Cre$^{TG/TG}$) mice and female (E, n=7 *Sst*-Cre$^{+/TG}$, n=7 *Sst*-Cre$^{TG/TG}$) mice, grouped by age. F and G) Glucose tolerance and quantification of the AUC-baseline of male (F, n=6 *Sst*-Cre$^{+/TG}$, n=3 *Sst*-Cre$^{TG/TG}$) and female (G, n=5 *Sst*-Cre$^{+/TG}$, n=5 *Sst*-Cre$^{TG/TG}$) mice. H) Plasma insulin levels before and 15 min after IP glucose administration in male mice (n=5 *Sst*-Cre$^{+/TG}$, n=4 *Sst*-Cre$^{TG/TG}$). I) Fold change in plasma insulin levels of male mice in H. J) Plasma insulin levels before and 15 min after IP glucose administration in female mice (n=6 *Sst*-Cre$^{+/TG}$, n=6 *Sst*-Cre$^{TG/TG}$). K) Fold change in plasma insulin levels of female mice in J. L and M) Static insulin secretion assay using islets from male (L, n=6 replicates, 10 islets each, pooled from 5 *Sst*-Cre$^{+/TG}$ or 4 *Sst*-Cre$^{TG/TG}$ mice) and female (M, n=4 replicates, 10 islets each, pooled from 6 *Sst*-Cre$^{+/TG}$ or 6 *Sst*-Cre$^{TG/TG}$ mice) mice incubated at 3 mM glucose and 11 mM glucose. Significance was determined by two-tailed unpaired t-test (B, AUC for F and G, I, K), one-way ANOVA followed by Holm-Sidak's adjustment for multiple comparisons (C), and two-way ANOVA or mixed modeling for genotype and time (D and E) or genotype and

glucose (F, G, H, J, L, M) followed by comparison of individual points by Holm-Sidak's adjustment multiple comparisons (E: *p=0.027). Error bars represent SEM.

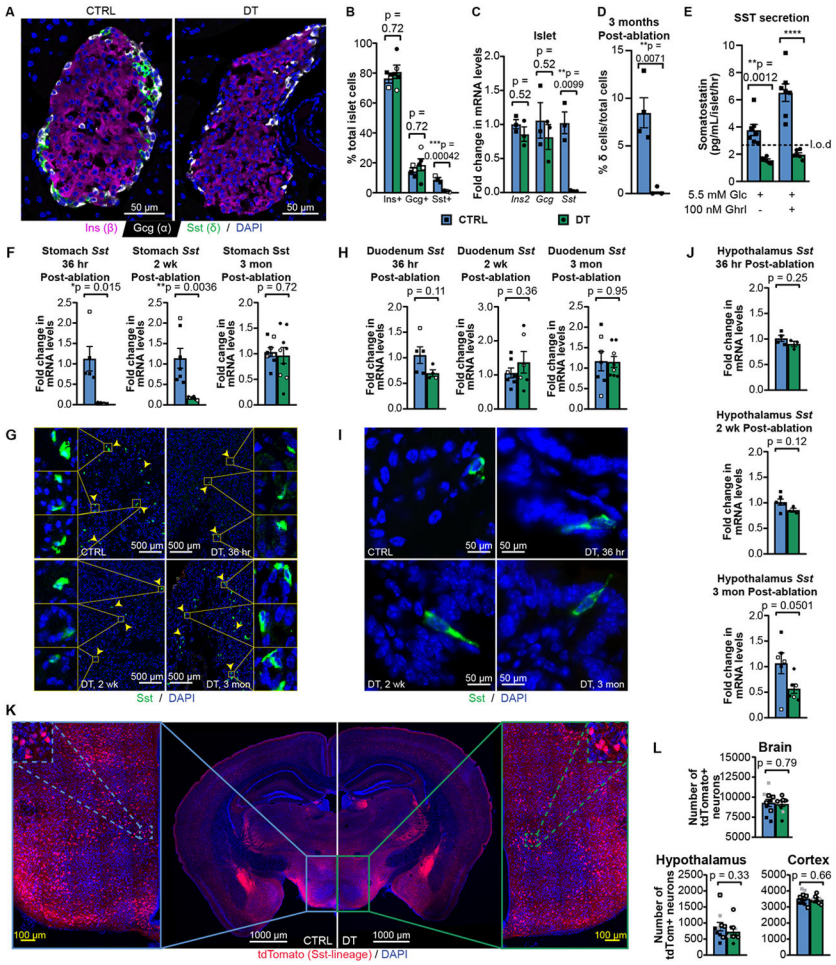

Fig. 2. Specific ablation of pancreatic δ cells in *Sst*-Cre x lsl-DTR mice.

A) Pancreas sections from control (CTRL) and δ cell-ablated (DT) mice. Scale bar represents 50 μm. B) Insulin, glucagon, and SST+ cell quantification (n=3 CTRL, n=5 DT). C) *Ins2, Gcg,* and *Sst* mRNA levels in islets from CTRL (n=3) and DT (n=3) mice. D) SST+ cell quantification 3 months post-ablation (n=4 CTRL, n=3 DT). E) SST secretion from CTRL (n=7 replicates, 30 islets each, pooled from 4 mice) and DT islets (n=6 replicates, 30 islets each, pooled from 4 mice) in 5.5 mM glucose +/− 100 nM ghrelin; l.o.d. = limit of detection. F and G) *Sst* mRNA levels (F) and SST stain (G) in stomach tissue collected 36 hours (n=5 CTRL, n=4 DT), 2 weeks (n=7 CTRL, n=6 DT), or 3 months (n=8 CTRL, n=9 DT) post-treatment. Yellow arrows indicate gastric D cells; yellow boxes indicate close-ups. Scale bars represent 500 μm. H and I) *Sst* mRNA levels (H) and SST stain (I) in duodenum tissue collected 36 hours (n=5 CTRL, n=4 DT), 2 weeks (n=7 CTRL, n=5 DT), or 3 months (n=7 CTRL, n=8 DT) post-treatment. J) *Sst* mRNA levels in hypothalamus collected 36 hours (n=4 CTRL, n=3 DT), 2 weeks (n=6 CTRL, n=3 DT), or 3 months (n=6 CTRL, n=6 DT) post-treatment. K) Brain cross-sections collected from *Sst*-Cre x lsl-tdTomato mice with (DT) or without lsl-DTR (CTRL) 36 hours post-DT, with close-ups of the hypothalamus region on the sides and further close-ups of neurons in the top corners. L) tdTomato+ neuron quantification in brain, hypothalamus, and cortex. 10 images from N=3 mice per group (represented by a black, gray, or open symbol) were quantified. Closed symbols

represent males and open symbols represent females in graphs. Significance was determined by multiple two-tailed unpaired t-tests followed by Holm-Sidak correction (B, C), two-tailed unpaired t-test (D, F, H, J, L), or two-way ANOVA followed by Holm-Sidak correction (E, ****$p<0.0001$). Error bars represent SEM.

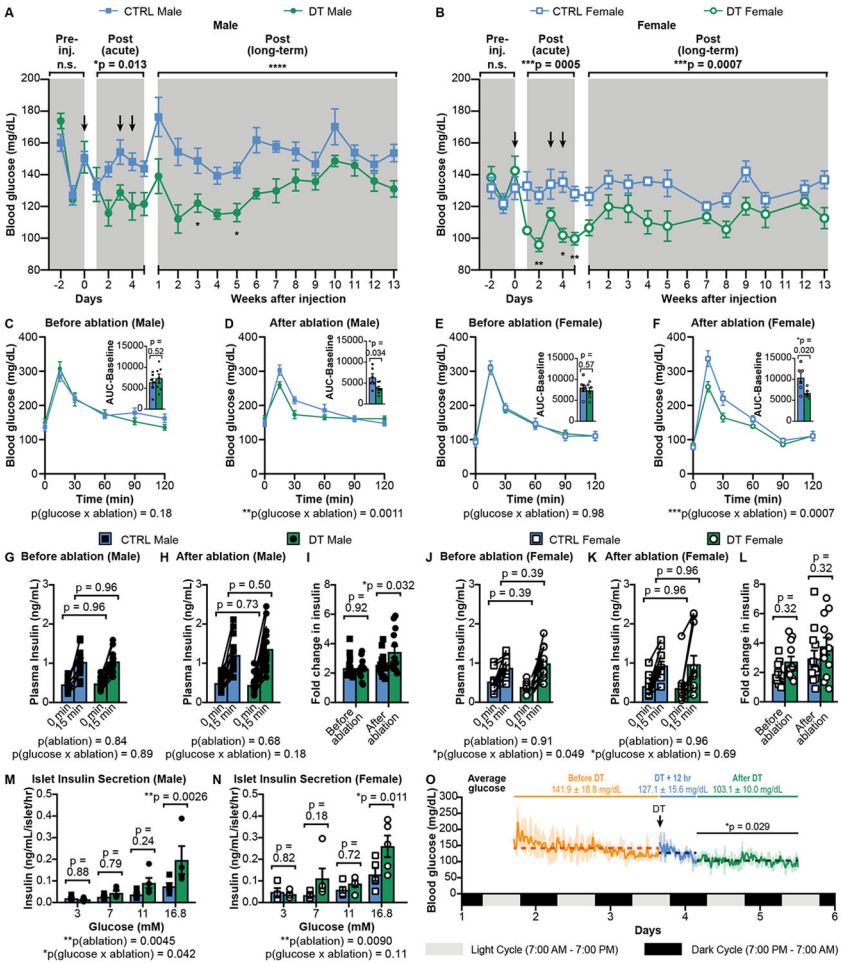

Fig. 3. δ cell ablation decreases the glycemic set point and increases glucose tolerance and insulin secretion.

A and B) Blood glucose measurements of male (A, n=8 CTRL, n=6 DT) and female (B, n=6 CTRL, n=6 DT) mice. Black arrows represent IP administration of SAL or DT. C-F) GTT of male mice (C-D: n=6 CTRL, n=7 DT) C) before and D) after δ cell ablation, and female mice (E-F: n=6 CTRL, n=6 DT) E) before and F) after δ cell ablation. Bar graphs in the upper right-hand corner of each line graph represent AUC-baseline. G-H) Plasma insulin measurements in male mice (n=15 CTRL, n=13 DT) G) before and H) after ablation. I) Fold change in plasma insulin levels between male CTRL and DT mice from G-H before and after ablation. J-K) Plasma insulin measurements in female mice (n=12 CTRL, n=12 DT) J) before and K) after ablation. L) Fold change in plasma insulin levels between female CTRL and DT mice from J-K before and after ablation. M and N) Static insulin secretion assay performed on islets isolated from ablated M) male (n=5 replicates per group, 10 islets each, pooled from 3 CTRL or 3 DT mice) and N) female (n=5 replicates per group, 10 islets each, pooled from 3 CTRL or 3 DT mice) mice. O) Averaged CGM data from n=3 mice. Orange represents glucose levels prior to single IP injection of DT. Blue represents when DT was administered and the 12 hours following. Green represents glucose levels measured 12 hours post-DT administration until the end of the experiment. Dashed lines represent average glucose level throughout each time period. Shaded regions around the line graph represent

SD. Significance was determined by two-way ANOVA for ablation (A, ****$p<0.0001$; B) or ablation and glucose (C-N, I, M, N) followed by Holm-Sidak's correction for multiple comparisons (A: *$p=0.026$, *$p=0.039$; B: **$p=0.0057$, *$p=0.012$, **$p=0.0057$), two-tailed unpaired t-test for AUC-baseline (C-F) or a one-way ANOVA of average glucose at baseline, DT, and after DT followed by Holm-Sidak's correction (O). Error bars represent SEM.

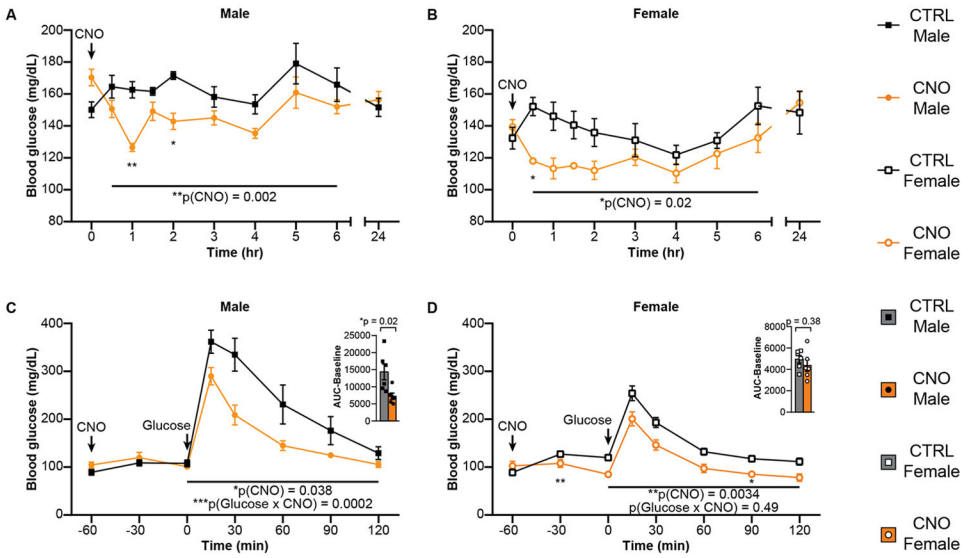

Fig. 4. Inhibition of δ cell activity decreases glycemia.

A and B) Hourly glucose measurements after administration of 1 mg/kg CNO at t = 0 min to A) male (n=6 CTRL, n=6 CNO) and B) female (n=6 CTRL, n=6 CNO) CNO-treated *Sst*-Cre x lsl-Gi-DREADD mice (CNO) or controls (CTRL). SAL-treated *Sst*-Cre x lsl-Gi-DREADD and CNO-treated *Sst*-Cre without lsl-Gi-DREADD mice were used as controls. C and D) GTT after 1 mg/kg CNO administration 1 hour before IP injection of glucose in male (C, n=6 CTRL, n=6 CNO) and female (D, n=6 CTRL, n=6 CNO) mice. Bar graphs in the upper right-hand corner of each line graph represent AUC-baseline. Significance was determined by two-way ANOVA for CNO (A, B) or glucose and CNO (C, D) followed by Holm-Sidak's correction for multiple comparisons (A: **p=0.0028, *p=0.010; B: *p=0.010; D: **p=0.0092, *p=0.031) and two-tailed unpaired t-test for AUC-baseline. Error bars represent SEM.

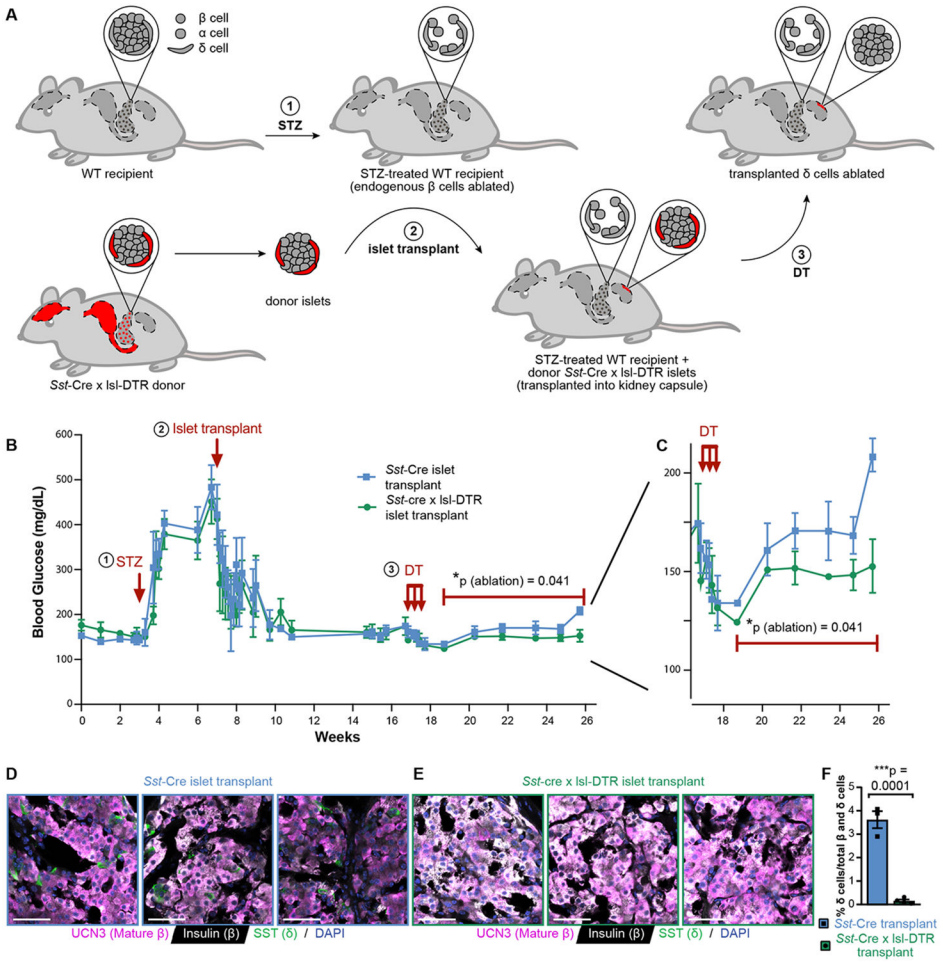

Fig. 5. Pancreatic δ cell ablation is sufficient to decrease the glycemic set point.

A) Schematic of the islet transplant strategy. 7 wild-type (WT) mice each received islets from a single donor (CTRL: n=3 WT receiving islets from *Sst*-Cre mice, DT: n=4 WT receiving islets from *Sst*-Cre x lsl-DTR mice). Outlines of the brain, stomach, gastrointestinal tract, pancreas, islets, and the kidney are shown within the mice. Red regions represent tissues in which DTR would be expressed in a *Sst*-Cre x lsl-DTR mouse. WT recipients were given 50 mg/kg of streptozotocin for 5 consecutive days (1). Islets were then isolated from *Sst*-Cre x lsl-DTR or control mouse donors and transplanted under the kidney capsule of the WT recipients (2). Only the δ within the transplanted islets express DTR in the recipient mice. After normoglycemia was re-established, the recipient mice with transplanted islets were administered 3 doses of DT as performed in the other experiments (3). B) Blood glucose measurements of the WT recipient mice throughout the course of the experiment. Blue lines represent recipients that received *Sst*-Cre islets (n=3) and green lines represent recipients that received *Sst*-Cre x lsl-DTR islets (n=4). C) An expanded view of the period during and after DT administration in B. D and E) Images of D) *Sst*-Cre only and E) *Sst*-Cre x lsl-DTR islets transplanted under the kidney capsule of WT mice. Scale bars represent 50 μm. F) Quantification of δ cells in *Sst*-Cre transplants (8,478 islet cells counted across n=3 mice) and *Sst*-Cre x lsl-DTR transplants (10,215 islet cells counted across n=4 mice). Significance was determined by two-way ANOVA for ablation followed

by Holm-Sidak's correction for multiple comparisons (B and C) and two-tailed unpaired t-test (F, ***p=0.0001). Error bars represent SEM.

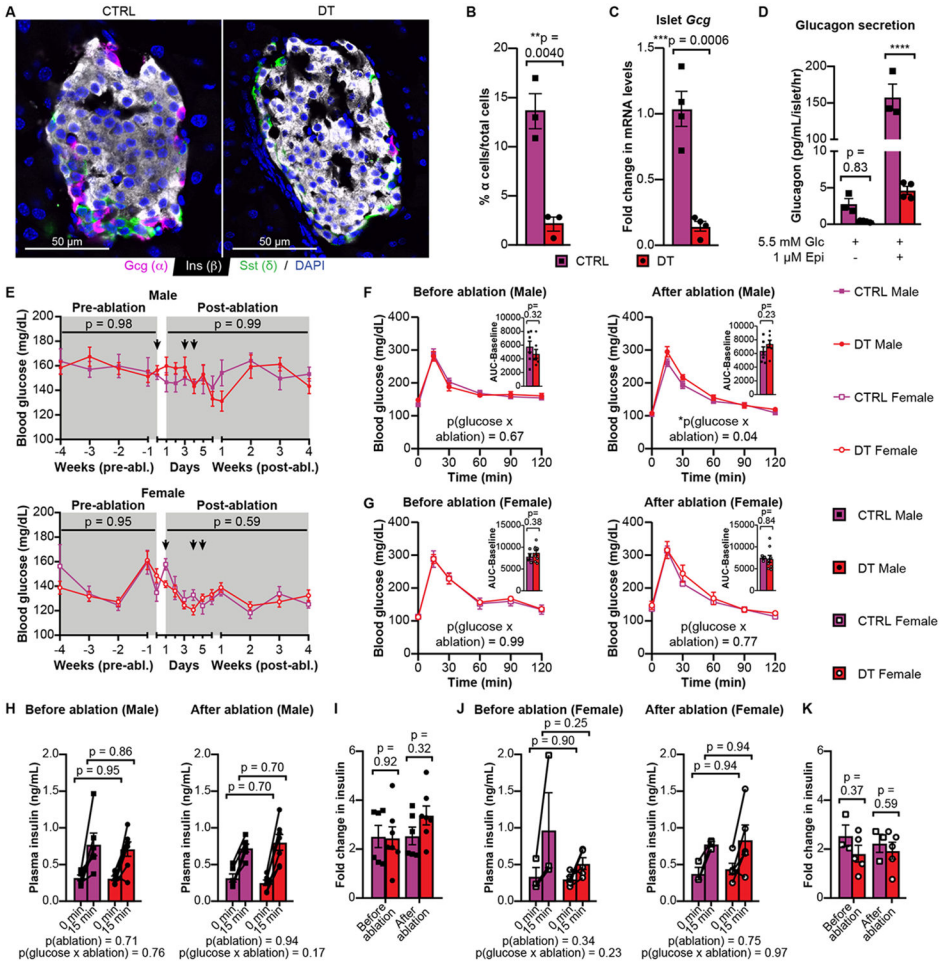

Fig. 6. α cell ablation does not affect basal glycemia.

A) Immunofluorescent stain of pancreas section from a non-ablated (left) and α cell-ablated mouse (right). Scale bar represents 50 μm. B) Quantification of α cell number (n=3 CTRL, n=3 DT). C) *Gcg* mRNA levels in islets from CTRL (n=4) and DT (n=4) mice. D) Glucagon secretion in CTRL (n=3 mice) and DT (n=4 mice) islets in the presence of 5.5 mM glucose +/− 1 μM epinephrine. E) Glucose measurements of male (top, n=5 CTRL, n=5 DT) and female mice (bottom, n=4 CTRL, n=10 DT). Arrows represent IP administration of DT. F and G) GTT in male (F, n=7 CTRL, n=7 DT) and female (G, n=4 CTRL, n=10 DT) mice before (left) and after (right) α cell ablation. Bar graphs in the upper right corner of each line graph represent AUC-baseline. H) Plasma insulin levels in male mice (n=6 CTRL, n=7 DT) before (left) and after (right) ablation. I) Fold change in plasma insulin levels between male CTRL and DT mice in H before and after administration of DT. J) Plasma insulin levels in female mice (n=3 CTRL, n=5 DT) before (left) and after (right) ablation. K) Fold change in plasma insulin levels between female CTRL and DT mice in J before and after administration of DT. Significance was determined by two-tailed unpaired t-test (B, C, AUC before and after ablation for F and G), two-way ANOVA for ablation and epinephrine (D, ****p<0.0001), ablation (E), or ablation and glucose (F-K) followed by Holm-Sidak's correction for multiple comparisons. Error bars represent SEM.

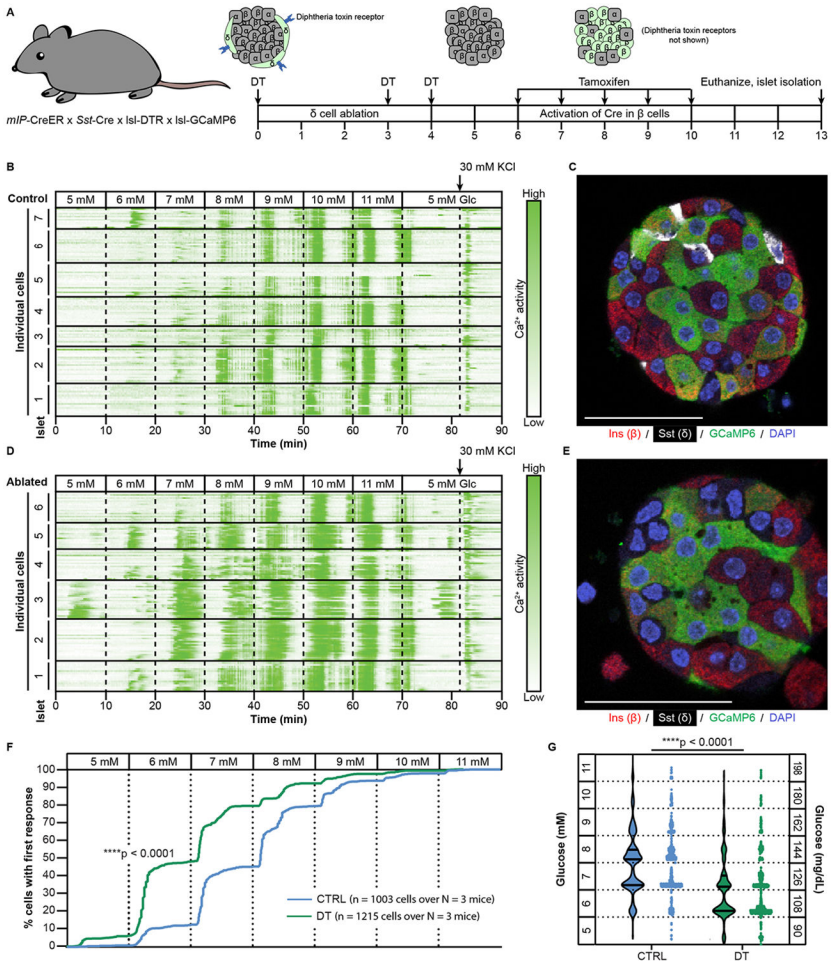

Fig. 7. β cells exhibit calcium response at a lower glucose threshold in the absence of δ cells.

A) Schematic of experimental design. B) Calcium traces from β cells in islets from a control mouse with intact pancreatic δ cells. C) *Post hoc* whole mount stain of an islet with intact δ cells. D) Calcium traces from β cells in islets from a mouse with ablated δ cells. E) *Post hoc* whole mount stain of an islet confirming absence of δ cells. Each line in panels B and D represents the calcium activity of a single β cell, with green intensity corresponding to an increase in intracellular calcium. Each box represents an islet. Dashed lines indicate the point at which the glucose levels were changed. Experiment was performed in n=3 mice (see Extended Data Fig. 5-7A). F) Curve representing the percentage that first respond at each glucose level. G) Violin plot in which each dot represents a cell and the glucose concentration to which it first responded. Significance was determined by Mantel-Cox test (F) and two-tailed unpaired t-test (G).

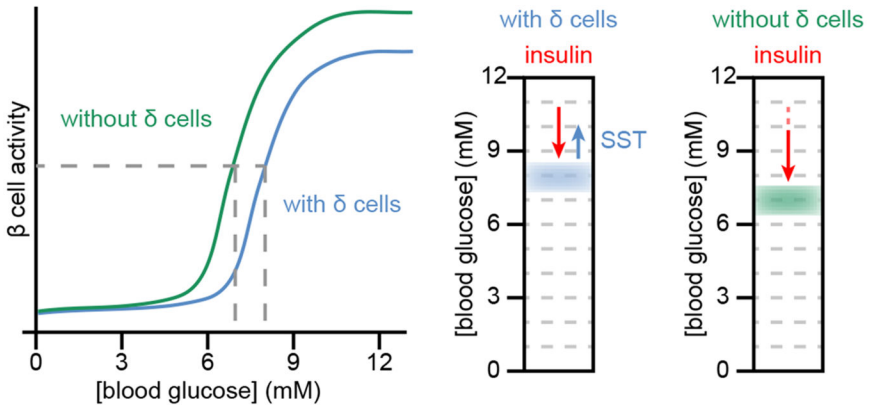

Fig. 8. Schematic of β cell glucose threshold and glycemic set point in the presence and absence of δ cells.

In the presence of δ cells, paracrine SST signaling pushes the β cell glucose threshold to the right, leading to a corresponding glycemic set point. When δ cells are removed, the absence of SST leads to a leftwards shift in the glucose threshold, leading to a corresponding decrease in the glycemic set point.